Pendrin inhibition as a novel diuretic strategy: targeting diuretic resistance and angiotensin II-induced hypertension

Kim, Gyuri

Department of
Graduate School
Yonsei University

Pendrin inhibition as a novel diuretic strategy: targeting diuretic resistance and angiotensin II-induced hypertension

Advisor Yoo, Tae Hyun

A Dissertation Submitted
to the Department of Medicine
and the Graduate School of Yonsei University
in partial fulfillment of the
requirements for the degree of
Doctor of Philosophy in Medical Science

Kim, Gyuri

June 2025

Pendrin inhibition as a novel diuretic strategy: targeting diuretic resistance and angiotensin II-induced hypertension

This certifies that the Dissertation
of Kim, Gyuri is approved

Committee Chair Han, Seung Hyeok

Committee Member Yoo, Tae Hyun

Committee Member Park, Sung Ha

Committee Member Namkung, Wan

Committee Member Kim, Dong Ki

Department of Medicine
Graduate School
Yonsei University
June 2025

TABLE OF CONTENTS

LIST OF FIGURES ·····iii
ABSTRACT IN ENGLISH ·····iv
1. INTRODUCTION·····1
2. MATERIALS AND METHODS·····3
2.1 Measurement of Cl^-/ HCO_3^- exchange activity in vitro·····3
2.2 Animal study ·····3
2.3 Blood and Urine Chemistry·····4
2.4 Cell study ·····4
2.5 Protein extraction ·····4
2.6 Total RNA extraction·····5
2.7 Real–time quantitative polymerase chain reaction·····5
2.8 Western blot analyses ·····6
2.9 Immunofluorescent staining ·····7
2.10 Library preparation and sequencing·····7
2.11 proximity-ligation assay (PLA)·····8
2.12 Statistical analyses ·····8
3. RESULTS ·····10
3.1 Comprehensive characterization of A4009, a novel pendrin inhibitor ·····10
3.2 Diuretic efficacy of a pendrin inhibitor in wild-type mice·····13
3.3 On-target specificity of pendrin inhibition in pendrin knockout mice ·····16
3.4 Diuretic efficacy of pendrin inhibitors was assessed in animal models with furosemide resistance model·····19
3.5 Diuretic efficacy of a pendrin inhibitor was assessed in angiotensin II-induced hypertensive models ·····23
3.6 Redistribution of tubular transporters in Furosemide resistance model·····27
3.7 Protein and mRNA expression of Sodium transporter in furosemide resistance model ·····30
3.8 Volcano plot of differentially expressed genes (DEGs) in furosemide treatment model ·····33
3.9 Protein-protein interaction in the furosemide resistance model·····35
3.10 Angiotensin II-mediated sodium transporter redistribution·····37
3.11. Protein and mRNA expression of sodium transporter in angiotensin II-induced hypertension model ·····40

3.12 Pendrin inhibition reduces on blood pressure in angiotensin II-induced hypertension model ……43
3.13 Regulation of Pendrin, Rac1, and NR3C2 mRNA by Aldosterone and Angiotensin II: Involvement of Rac1 and MR Signaling ……45
3.14 Pendrin-Rac1 interaction in collecting duct cells is enhanced by angiotensin II and aldosterone ……47
4. DISCUSSION ……49
5. CONCLUSION……53
REFERENCES ……54
ABSTRACT IN KOREAN ……57

LIST OF FIGURES

<Fig 1> Characterization of A4009 as a Novel Pendrin Inhibitor ····· 11
<Fig 2> Effects of pendrin inhibition on urine output and electrolyte excretion in the wild type mice ····· 15
<Fig 3> Effects of a pendrin inhibitor on urine Output and electrolyte excretion in pendrin knockout mice ····· 18
<Fig 4> Effects of pendrin inhibition on urine output and electrolyte excretion in the furosemide resistant model ····· 22
<Fig 5> Effects of pendrin inhibition on urine output and electrolyte excretion in angiotensin II-induced hypertensive models ····· 26
<Fig 6> Immunofluorescence analysis of sodium transporter expression and localization in furosemide resistant model. ····· 29
<Fig 7> Protein and mRNA expression of sodium transporters in Furosemide resistance model ····· 32
<Fig 8> Volcano plot of differentially expressed genes (DEGs) ····· 34
<Fig 9> Protein-protein interaction (PPI) network analysis ····· 36
<Fig 10> Immunofluorescence analysis of sodium transporter expression and localization in the angiotensin II-induced model ····· 39
<Fig 11> Protein and mRNA expression of sodium transporter in angiotensin II-induced hypertension model ····· 42
<Fig 12> Effect of pendrin inhibition on blood pressure in angiotensin II-induced hypertension model ····· 44
<Fig 13> mRNA expression levels of pendrin, Rac1 and NR3C2 in mouse collecting duct cells under treatment conditions ····· 46
<Fig 14> Proximity ligation assay (PLA) analysis of pendrin-Rac1 interaction in mouse collecting duct cells ····· 48

ABSTRACT

Pendrin inhibition as a novel diuretic strategy: targeting diuretic resistance and angiotensin II-induced hypertension

Background : Pendrin (SLC26A4) is an anion exchanger that plays a role in sodium chloride and water reabsorption in the kidney. It is localized to the apical membrane of β-intercalated and non-A/non-B intercalated cells in the connecting tubule and cortical collecting duct. Pendrin primarily mediates chloride reabsorption and bicarbonate secretion via Cl^-/HCO_3^- exchange and indirectly influences sodium reabsorption by modulating the epithelial sodium channel (ENaC) and the Na^+-dependent Cl^-/HCO_3^- exchanger (NDCBE). Recent studies have demonstrated an interaction between pendrin and the Na-K-Cl cotransporter (NKCC2), showing that simultaneous inhibition of both transporters results in a potent diuretic effect in experimental models. This study aims to investigate the effects of a novel pendrin inhibitor on diuretic resistance, particularly under conditions of pendrin upregulation. To further evaluate the role of angiotensin II in this process, An angiotensin II-induced hypertension model is employed to investigate the pathophysiological context, and the synergistic diuretic effects of furosemide in combination with pendrin inhibitors are evaluated as a potential therapeutic strategy.

Method : In vitro Cl^-/HCO_3^- exchange activity was measured in pendrin-overexpressing PANC-1 cells using a pH-sensitive fluorescent dye following treatment with A4009. diuretic efficacy was tested in wild-type mice, a furosemide-resistant model, and an angiotensin II-induced hypertensive model. Urine output and electrolyte excretion were measured to assess the effects of A4009 alone and in combination with furosemide. In the angiotensin II-induced model, blood pressure was also measured. To elucidate the molecular mechanisms underlying pendrin pathway activation, the mRNA and protein expression levels of key sodium transporters and regulatory molecules were quantitatively evaluated in each animal model using real-time quantitative PCR (qPCR) and western blot analysis. Furthermore, Proximity Ligation Assay (PLA) and mRNA sequencing were conducted to elucidate the molecular interactions between pendrin and its associated signaling proteins.

Result : A novel pendrin inhibitor, A4009, was identified through in vitro screening and evaluated for its inhibitory effects on pendrin-mediated Cl^-/I^- and Cl^-/HCO_3^- exchange, yielding IC_{50} values of 59.5 ± 12.8 nM and 52.6 ± 15.7 nM, respectively. In wild-type mice, the co-administration of furosemide and A4009 led to a significant dose-dependent increase in urine output. This increase was accompanied by a significant rise in sodium (Na^+) and chloride (Cl^-) excretion compared to furosemide alone. While A4009 monotherapy had no effect on potassium (K^+) excretion, co-administration with furosemide resulted in a significant increase. Additionally, urinary osmolality was significantly reduced in the combination groups, indicating enhanced urine dilution capacity. In the furosemide-resistant model, A4009 monotherapy modestly increased urine output, and co-administration with furosemide significantly increased urine output. Co-administration further increased Na^+, Cl^-, and K^+ excretion and significantly decreased urine osmolality. This effect was

associated with increased pendrin, Rac1, and NR3C2 expression, suggesting a functional link between pendrin activity and Rac1 signaling in diuretic resistance. The diuretic efficacy of A4009 was further confirmed in the angiotensin II-induced hypertension model. A4009 monotherapy did not significantly affect urine volume or electrolyte excretion, but co-administration with furosemide significantly increased urine output and electrolyte excretion, while reducing urine osmolality. A4009 alone effectively reduced blood pressure in hypertensive mice. This suggests that pendrin inhibition enhances the diuretic response and contributes to blood pressure reduction in hypertensive conditions.

Conclusion : These findings suggest that pendrin inhibition may be effective in mitigating sodium and water retention under conditions of angiotensin II-induced hypertension and diuretic resistance. Our results highlight the potential of pendrin inhibitors as novel diuretic candidates, particularly in conditions where pendrin expression is upregulated. Future studies should further assess the long-term safety and efficacy of A4009 in pendrin-overexpressing models and explore its therapeutic applications in diverse pathophysiological conditions to expand its clinical relevance.

Key words : diuretic, diuretic resistance, RAAS system, Pendrin, AngiotensinII

1. INTRODUCTION

Diuretic resistance remains a major challenge in managing fluid overload in the patients with heart failure and chronic kidney disease. Long-term loop diuretic therapy often leads to a diminished natriuretic response due to compensatory sodium reabsorption in the kidney [1]. Emerging evidence suggests that pendrin (SLC26A4), a Cl^-/ HCO_3^- exchanger in the renal cortical collecting duct, plays a critical role in this process by modulating sodium transport mechanisms [2-6]. A recent study has revealed that pendrin possesses an asymmetric homodimeric structure, consisting of one inward-facing protomer and one outward-facing protomer [7]. This unique structural arrangement enables pendrin to simultaneously mediate both anion absorption and secretion, which is fundamental to its role as an electrically neutral exchanger [8]. Pendrin expression is dynamically regulated by physiological and pathological stimuli. It is upregulated in response to aldosterone, chloride restriction, and metabolic alkalosis and downregulated by chloride loading and metabolic acidosis [6, 9-11]. These regulatory mechanisms involve changes in mRNA expression, protein abundance, intracellular localization, and the number of pendrin-expressing cells in the collecting duct. A clinical condition in which pendrin is upregulated, plays a role is diuretic resistance, particularly less responsive to furosemide as a loop diuretic. Long-term furosemide use often leads to compensatory sodium reabsorption in the downstream nephron, notably in the collecting duct, reducing its diuretic efficacy [12, 13]. The main mechanisms contributing to diuretic resistance include decreased renal blood flow, reduce diuretic secretion in the proximal tubule, and decrease glomerular filtration rate. Moreover, the activation of compensatory mechanisms, including increased sodium reabsorption via pendrin and the epithelial sodium channel (ENaC), is a key contributor to diuretic resistance. The renin-angiotensin-aldosterone system (RAAS) and angiotensin II signaling have been widely recognized as major regulators of sodium homeostasis. ENaC and Na^+-Cl^- Cotransporter (NCC) have been well established as key sodium transporters in this pathway.

This suggests that targeting pendrin could serve as a novel diuretic strategy to mitigate RAAS-mediated sodium retention, particularly in diuretic resistance. The RAAS also plays a critical role in regulating blood pressure through controlling fluid homeostasis and vascular constriction [7, 14].

To investigate the role of pendrin in these conditions, I utilized two experimental models which are upregulated in pendrin expression.

First, the long-term furosemide administration model is first employed to mimic the diuretic-resistant state observed in clinical settings [12]. In this model, it was reported that

pendrin expression increases due to the activation of compensatory mechanisms in the kidney [3, 15]. This model can provide an opportunity to study the potential of pendrin inhibitors in overcoming diuretic resistance[16-18].

The second model is the angiotensin II-induced model, which activates the RAAS and increases pendrin expression. Angiotensin II promotes sodium reabsorption in the kidney along with blood pressure elevation.

The development of pendrin inhibitors is gaining attention as a new diuretic treatment strategy to overcome furosemide resistance [9, 19]. According to Verkman et al., pendrin inhibitors alone did not show a diuretic effect but synergistically enhanced the diuretic effect when combined with furosemide. Particularly in a mouse model where pendrin was upregulated in the kidney due to long-term furosemide treatment, pendrin inhibitors increased urine output by 60% [19].

To address the role of pendrin in diuretic resistance, two experimental models of pendrin overexpression are employed. These models are used to assess the efficacy of pendrin inhibitors, both as monotherapy and in combination with furosemide, in overcoming diuretic resistance.

2. MATERIALS AND METHODS.

2.1 Measurement of Cl^-/ HCO_3^- exchange activity in vitro

A stable PANC-1 cell line overexpressing pendrin (PDS-expressing PANC-1) was generated and maintained as previously described[20]. The intracellular pH of PDS-expressing PANC-1 cells was measured using the pH-sensitive fluorescent probe 2′,7′-bis-(2-carboxyethyl)-5-(and-6)-carboxyfluorescein. A4009 was used to inhibit pendrin activity, while 4,4′-diisothiocyanatostilbene-2,2′-disulfonic acid (DIDS) was used as a general anion exchanger inhibitor. Six hours after A4009 treatment, intracellular pH was measured as previously described, followed by the acute addition of 0.1 mM DIDS and continuous measurement.

2.2 Animal study

All animal experiments adhered to a protocol approved by the Committee for the Care and Use of Laboratory Animals of Yonsei University College of Medicine. Six-week-old male C57BL/6 wild-type (WT) mice and pendrin knockout mice were used in this study. Pendrin KO mice were generously provided by Dr. JY Choi[21]. Mice were assigned to four experimental groups: Wild type, pendrin KO, furosemide treatment (Furosemide, Sigma-Aldrich, St. Louis, MO), and angiotensin II treatment (Angiotensin II, Sigma Chemical Co., St. Louis, MO, USA)

Furosemide treatment group: A furosemide resistance model was established as follows. High-dose furosemide (20 mg/kg, twice daily; total daily dose: 40 mg/kg/day) was administered via intraperitoneal (I.P.) injection for 10 days.

Angiotensin II treatment group: angiotensin II was continuously delivered at 1400 μg/kg/day for two weeks via Alzet osmotic pumps (Alzet 1002, Durect Corporation) implanted subcutaneously. Blood pressure was measured noninvasively using the BP-2000 Blood Pressure Analysis System (Visitech Systems) at the second week of infusion. Measurements were performed between 1 PM and 5 PM over three consecutive days, with each session consisting of two sets of 10 readings per mouse. Urine samples were collected and urine volume was measured over a 6-hour period using metabolic cages following intraperitoneal drug administration.Mice were sacrificed after four weeks of treatment. Mice were anesthetized with Zoletil (Virbac, Carros, France) at 10 mg/kg, and 300–500 μL of blood was collected from the heart following a central line incision. The kidneys were extracted while the animals were still under anesthesia, immediately frozen in liquid nitrogen, and stored at -80°C until use.

2.3 Blood and urine chemistry

Urinary electrolyte concentrations, including sodium (Na^+), potassium (K^+), and chloride (Cl^-), were measured using an indirect ion-selective electrode analyzer (SCL Lab, Seoul, Republic of Korea). Urine osmolality was assessed with a freezing-point depression osmometer (Advanced 2020, Advanced Instruments, USA). To evaluate renal function, serum blood urea nitrogen (BUN) and creatinine (Cr) levels were quantified using a commercially available automated biochemistry analyzer (Hitachi 7180, Hitachi High-Technologies, Tokyo, Japan).

2.4 Cell study

Mouse collecting duct (mCD) cells were cultured in DMEM/F-12 medium supplemented with 10% fetal bovine serum (FBS) and 1% penicillin-streptomycin at 37°C in a humidified incubator with 5% CO_2 . Cells were treated with aldosterone (1 μM), angiotensin II (1 μM), spironolactone (10 μM), and Rac1 inhibitor NSC23766 (50 μM) for the indicated time points to investigate the regulation of pendrin and Rac1 expression.

2.5 Protein extraction

Proteins were extracted from cells and kidney tissue using RIPA lysis and extraction buffer supplemented with protease inhibitors. Samples were homogenized, kept on ice, and centrifuged at 14,000 × g for 15 minutes at 4℃. The supernatant was collected, and protein concentration was determined using the BCA assay.

2.6 Total RNA extraction

Total RNA was extracted from whole kidney tissues using a modified guanidinium thiocyanate–phenol–chloroform protocol. Kidney samples were initially homogenized in 700 μl of RNAiso solution with a mortar and pestle, repeating the process three times to ensure thorough disruption. Following homogenization, 160 μl of chloroform was added to the mixture, which was then vortexed for 30 seconds and incubated at room temperature for 3 minutes. The samples were centrifuged at 12,000 × g for 15 minutes at 4°C, and the resulting upper aqueous phase was transferred to a new RNase-free microtube. RNA was precipitated by mixing the aqueous layer with 500 μl of isopropanol and centrifuging again at 12,000 × g for 30 minutes at 4°C. The resulting RNA pellet was rinsed with 70% ethanol, briefly air-dried, and dissolved in DEPC-treated water. The yield and purity of RNA were determined by measuring the absorbance at 260 and 280 nm using a NanoDrop spectrophotometer (Thermo Fisher Scientific). To evaluate RNA integrity, samples were

analyzed by agarose gel electrophoresis, with visual confirmation of 28S and 18S ribosomal RNA bands.

2.7 Real–time quantitative polymerase chain reaction

Complementary DNA (cDNA) was synthesized from total RNA using the PrimeScript™ First Strand cDNA Synthesis Kit (Takara Bio, Kusatsu, Japan), following the protocol provided by the manufacturer. Quantitative real-time PCR (RT-qPCR) was subsequently carried out on a QuantStudio™ 3 Real-Time PCR System (Applied Biosystems, Foster City, CA, USA). For amplification, gene-specific primers targeting pendrin, NKCC2, NCC, ENaC, RAC1, and GAPDH were utilized from the PrimePCR™ PreAmp Probe Assay kit (Bio-Rad Laboratories, Kabelsketal, Germany). Each PCR reaction contained 2 μl of cDNA template, 10 μl of SsoAdvanced™ Universal Probes Supermix (Bio-Rad), 1 μl of the 20× PrimePCR™ assay, and nuclease-free water, adjusted to a total reaction volume of 20 μl. The thermal protocol included an initial denaturation step at 95°C for 30 seconds, followed by 40 amplification cycles comprising 15 seconds at 95°C and 60 seconds at 60°C for annealing and extension. All reactions were performed in triplicate to ensure reproducibility. Relative mRNA expression levels were analyzed using the $2^{\wedge(-\Delta\Delta Ct)}$ method, with GAPDH serving as the endogenous reference gene. Melting curve analysis was performed to validate the specificity of the amplification products.

2.8 Western blot analyses

Protein samples (30–50 μg per lane) were subjected to separation by SDS-polyacrylamide gel electrophoresis (SDS-PAGE) using 10–12% gels, followed by electrotransfer onto PVDF membranes (Millipore, Bedford, MA, USA) using a wet transfer apparatus. To block non-specific binding, the membranes were incubated in 5% non-fat milk dissolved in Tris-buffered saline with 0.1% Tween 20 (TBST) for 1 hour at room temperature. After blocking, membranes were incubated overnight at 4°C with primary antibodies diluted in TBST containing 5% bovine serum albumin (BSA). The antibodies used included: anti-Pendrin (PA5-42060, Thermo Fisher Scientific, Rockford, IL, USA), anti-NKCC2 (LS-C430323, LSBio, Seattle, WA, USA), anti-NCC (Abcam, Cambridge, MA, USA), anti-ENaC α (NB100-74357, Novus Biologicals, Littleton, CO, USA), anti-Rac1 (#4651, Cell Signaling Technology, Danvers, MA, USA), anti-AGTR1 (PA5-20812, Thermo Fisher Scientific, Rockford, IL, USA), and anti-β-actin (A2228, Sigma-Aldrich, St. Louis, MO, USA), which served as a loading control. Following extensive washing with TBST, the membranes were exposed to horseradish peroxidase (HRP)-conjugated secondary antibodies (anti-mouse, anti-rabbit, or anti-goat IgG; GenDEPOT, Baker, TX) for 1 hour at ambient temperature, selected based on the species of the primary antibody. Protein detection was carried out

using an enhanced chemiluminescence (ECL) system (Amersham Life Science, Loughborough, UK). The intensity of the protein bands was measured using ImageJ software (NIH, Bethesda, MD, USA), and expression levels of target proteins were normalized against β-actin as the internal control.

2.9 Immunofluorescent staining

Immunofluorescence staining was carried out on 3 μm-thick paraffin-embedded tissue sections mounted onto slides pre-coated with paraffin. After deparaffinization and rehydration, antigen retrieval was performed by heating the sections in 10 mM sodium citrate buffer (pH 6.0) using a microwave oven. To minimize nonspecific binding, tissue sections were incubated with 5% normal donkey serum for 30 minutes at room temperature. Subsequently, the sections were incubated overnight at 4°C with primary antibodies diluted in blocking buffer. The following antibodies were used: anti-Pendrin (PA5-42060, Thermo Fisher Scientific, Rockford, IL, USA), anti-NKCC2 (#38436, Cell Signaling Technology, Danvers, MA, USA), anti-NCC (Abcam, Cambridge, MA, USA), anti-ENaC α (NB100-74357, Novus Biologicals, Littleton, CO, USA). On the next day, slides were incubated with a fluorescently labeled secondary antibody (anti-rabbit Alexa Fluor 488, Abcam, Cambridge, MA, USA), and nuclei were counterstained with DAPI. Imaging was performed using a confocal microscope (LSM700, Carl Zeiss Vision, Hallbergmoos, Germany) at 40× magnification. For quantitative analysis, immunofluorescence signal was measured using ImageJ software (NIH, Bethesda, MD, USA). A minimum of 20 randomly selected fields per sample were analyzed, and the immunopositive area was expressed as a percentage of the total tissue area.

2.10 Library preparation and sequencing

To explore gene expression alterations, RNA sequencing was performed using kidney tissues collected from both control and furosemide-resistant mice. Total RNA was extracted, and sequencing libraries were constructed using the CORALL RNA-Seq V2 Library Preparation Kit (LEXOGEN, Austria), following the manufacturer's guidelines. Messenger RNA (mRNA) was isolated using the Poly(A) RNA Selection Kit (LEXOGEN), after which complementary DNA (cDNA) was synthesized and fragmented enzymatically. Sample indexing was carried out using Illumina indexes 1 through 12, and the resulting libraries were amplified via PCR for enrichment. To evaluate library integrity and size distribution, the TapeStation system with High Sensitivity D1000 ScreenTape (Agilent Technologies, Netherlands) was used. Quantification of the final libraries was performed via real-time PCR using the StepOne Real-Time PCR System (Applied Biosystems, USA). Sequencing was conducted on the Illumina NovaSeq 6000 platform in a paired-end 100 bp

mode to ensure high coverage and read accuracy. For bioinformatic analysis, the quality of raw sequencing reads was assessed with FastQC, and trimming of adapter sequences and low-quality bases was handled using Fastp. The processed reads were aligned to the reference genome with STAR, and transcript abundance was estimated using Salmon. Normalization of read counts was performed using the Trimmed Mean of M-values (TMM) method followed by counts per million (CPM), implemented via the EdgeR package. Downstream analysis, including differential gene expression and data visualization, was conducted using ExDEGA software (Ebiogen Inc., Korea).

2.11 proximity-ligation assay (PLA)

To investigate the interaction between Pendrin and Rac1, a proximity ligation assay (PLA) was performed using the DuoLink® In Situ Detection Kit (Sigma-Aldrich, USA). The M-1 cell line (ATCC® CRL-2038™), a murine cortical collecting duct cell line, was obtained from the American Type Culture Collection (ATCC, Manassas, VA, USA) and used for this analysis. Cells were first fixed and permeabilized using 0.25% Triton X-100, followed by incubation with DuoLink blocking buffer at 37°C for 1 hour in a humidified chamber to prevent non-specific antibody binding. Subsequently, mouse monoclonal anti-Pendrin and rabbit polyclonal anti-Rac1 primary antibodies were applied, and cells were incubated overnight at 4°C. After rinsing three times with buffer A, DuoLink PLA Plus and Minus probes—species-specific secondary antibodies conjugated to oligonucleotides—were added and incubated at 37°C for 1 hour. Ligation of the proximity probes was then carried out using DNA ligase, and signal amplification was performed using DNA polymerase. Following the amplification step, cells were washed with buffer B, counterstained with DAPI, and mounted using DuoLink In Situ Mounting Medium. Fluorescent signals were visualized using a Zeiss LSM 510 Meta confocal microscope. Quantification of PLA puncta (representing protein–protein interactions) was carried out using ImageJ software, with analysis conducted in both the cytoplasmic and nuclear compartments.

2.13 Statistical analyses

Statistical analyses were performed using GraphPad Prism version 10.3.1 (GraphPad Software Inc., La Jolla, CA, USA). Significance was determined using a two-tailed unpaired Student's t-test for comparisons between two groups or a one-way or two-way analysis of variance (ANOVA) with Tukey's multiple comparisons test for comparisons involving multiple groups. All data are presented as means ± SEM, and a p-value less than 0.05 was considered statistically significant.

3. RESULT

3.1 Comprehensive characterization of A4009, a novel pendrin inhibitor

A 4009 as a novel pendrin inhibitor selected from a cell-based YFP fluorescence quenching assay was characterized in vitro (Figure 1). The inhibitory effect of A4009 on pendrin-mediated anion exchange was evaluated using LN215 cells stably expressing human pendrin. These cells lack endogenous anion transport activity, enabling the measurement of pendrin-specific activity without background interference. A4009 inhibited Cl^-/I^-, Cl^-/SCN^-, and Cl^-/HCO_3^- exchange, with IC_{50} values of 59.5 ± 12.8, 55.2 ± 5.7, and 52.6 ± 15.7 nM, respectively (Figure 1A). To assess A4009's effect on mouse pendrin, I examined anion exchange in LN215 cells expressing mouse pendrin. A4009 inhibited mouse pendrin-mediated anion exchange, with IC_{50} values of 0.9 ± 0.1, 1.3 ± 0.1, and 0.5 ± 0.04 μM for Cl^-/I^-, Cl^-/SCN^-, and Cl^-/HCO_3^- exchange, respectively (Figure 1B). To evaluate the selectivity of A4009, I tested its effects on other human SLC26 family members (SLC26A3, SLC26A6, SLC26A7, and SLC26A9) as well as chloride channels (CFTR and ANO1). At 10 μM, A4009 exhibited no significant inhibition of SLC26A7, SLC26A9, CFTR, or ANO1 (Figure 1C). However, A4009 showed weaker inhibition of SLC26A3 (IC_{50} = 378 ± 33.5 nM) and SLC26A6 (IC_{50} = 3.9 ± 0.6 μM) compared to its effect on pendrin (IC_{50} = 59.5 ± 12.8 nM). The inhibitory effect of A4009 on pendrin-mediated Cl^-/HCO_3^- exchange was further assessed using human WT pendrin-overexpressing PANC-1 cells. To exclude AE1-related effects, 0.1 mM DIDS was used. A4009 inhibited pendrin activity by 79.3% and 88.1% (P = 0.017) at 10 and 30 μM, respectively, after 6 hours of treatment (Figure 1D). To assess cytotoxicity, MTS assays were performed on NRK-49F and NRK-52E of rat kidney cell lines. A4009 exhibited no significant cytotoxicity at 100 μM. In contrast, other pendrin inhibitors (PDSinh-A01, PDSinh-C01, and YS-01) reduced cell viability as the dose increased, with PDSinh-C01 nearly eliminating viability at 10 μM in both cell lines (Figure 1E, F). To assess cytotoxicity, MTS assays were performed on NRK-49F and NRK-52E of rat kidney cell lines. A4009 exhibited no significant cytotoxicity at 100 μM. In contrast, other pendrin inhibitors (PDSinh-A01, PDSinh-C01, and YS-01) reduced cell viability as the dose increased, with PDSinh-C01 nearly eliminating viability at 10 μM in both cell lines (Figure 1E, F).

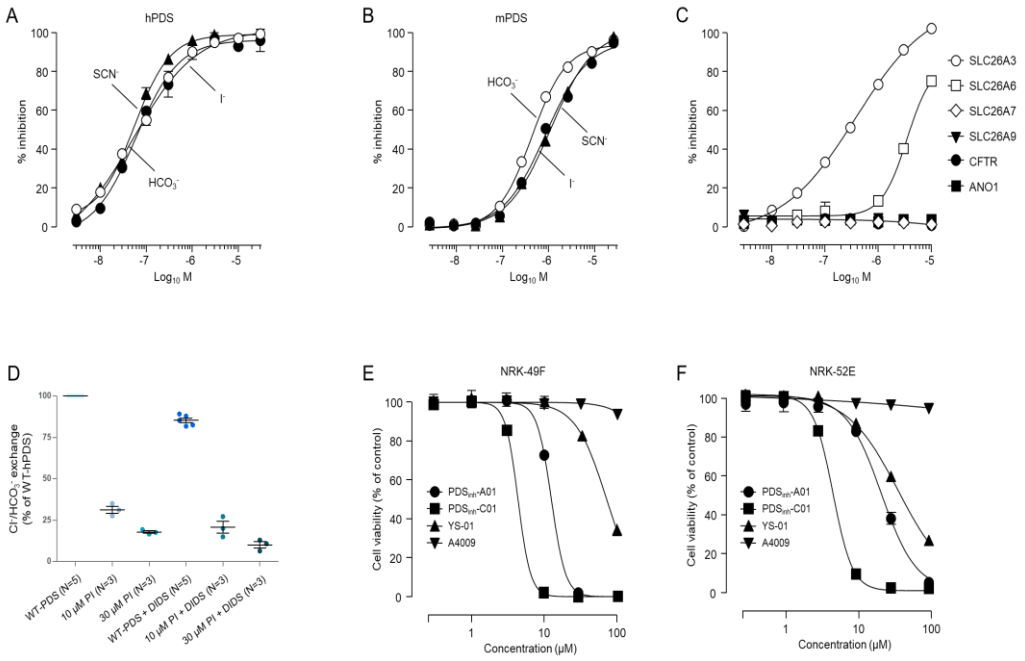

Figure 1. Characterization of A4009 as a novel pendrin inhibitor

(A, B) Inhibition of pendrin-mediated anion exchange – The dose-dependent effects of A4009 on Cl^-/anion exchange activity were evaluated in LN215 cells expressing human pendrin (A, N = 6) and mouse pendrin (B, N = 6), demonstrating a concentration-dependent inhibition. (C) Selectivity Profile of A4009 – The inhibitory effects of A4009 on other SLC26 family members (SLC26A3, A6, A7, and A9) and chloride channels (CFTR and ANO1) were evaluated, showing minimal off-target effects. (C, N = 6 for each target).

(D) Suppression of Cl^-/HCO_3^- Exchange in PANC-1 Cells – A4009 treatment (10 μM and 30 μM) significantly inhibited Cl^-/HCO_3^- exchange by 68.7% and 82.8%, respectively, in PANC-1 cells stably expressing wild-type human pendrin (D, N = 4 for control; N = 3 for each treatment group). The inhibitory effect of A4009 was not altered by co-treatment with DIDS, which resulted in comparable suppression (WT-PDS + DIDS: 14.7%; 10 μM A4009: 79.3%; 30 μM A4009: 88.1%). (E, F) Cytotoxicity Evaluation in Kidney Cell Lines – The cytotoxic effects of A4009, PDSinh-A01, PDSinh-C01, and YS-01 were examined in NRK-49F (E) and NRK-52E (F) kidney cell lines following 24-hour treatment. Cell viability was assessed using the MTS colorimetric assay. A4009 showed lower cytotoxicity compared to other pendrin inhibitors (N = 6 for each condition).

Statistical analysis was performed using the Kruskal–Wallis test. Statistical significance was determined as follows: $*p < 0.05$; All data are presented as mean ± SEM

3.2 Diuretic efficacy of a pendrin inhibitor in wild-type mice

Urine output and electrolyte excretion were measured to assess the diuretic efficacy of pendrin inhibition in wild-type mice treated with furosemide and A4009 (Figure 2). Furosemide significantly increased urine output compared to the control ($p < 0.0001$), while A4009 alone had no effect on urine output. A4009 co-treatment with furosemide significantly and dose-dependently elevated urine output ($p < 0.0001$), indicating a potentiated diuretic effect (Figure 2A). Electrolyte analysis revealed that urinary sodium (Na^+) and chloride (Cl^-) excretion were significantly elevated by furosemide alone ($p < 0.0001$), and this effect was further increased with higher doses of A4009 when co-administered ($p < 0.0001$), suggesting that pendrin inhibition enhances furosemide-induced sodium and chloride excretion in urine (Figure 2B, D). Urinary potassium (K^+) excretion was also elevated in furosemide-treated mice ($p = 0.0023$), and further increased when A4009 was added ($p < 0.0001$), suggesting enhanced urinary potassium excretion (Figure 2C). Urine osmolality was significantly reduced in the furosemide-treated group compared to the control ($p < 0.0001$), indicating urine dilution. While A4009 alone did not alter urine osmolality, its co-administration with furosemide led to a progressively greater reduction in osmolality as the A4009 dose increased ($p < 0.0001$), confirming enhanced urinary dilution (Figure 2E). These findings indicate that pendrin inhibition augments the diuretic response to furosemide, increasing sodium, chloride, and potassium excretion while improving urine output, highlighting its potential therapeutic role in enhancing loop diuretic efficacy.

A

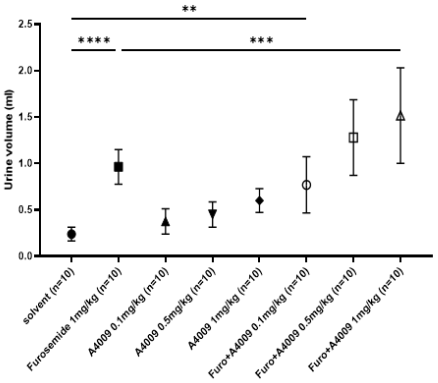

B

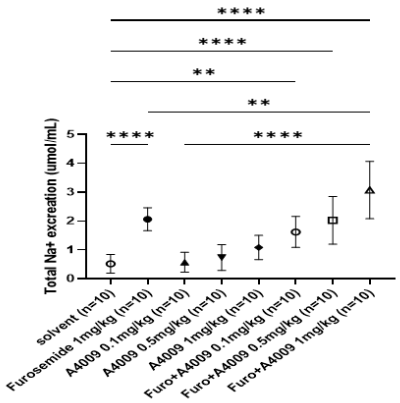

C

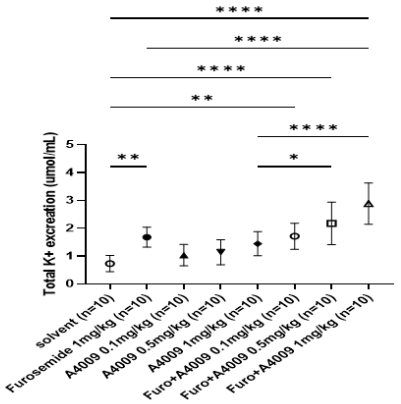

D

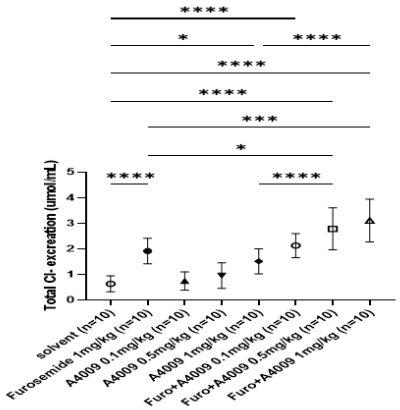

E

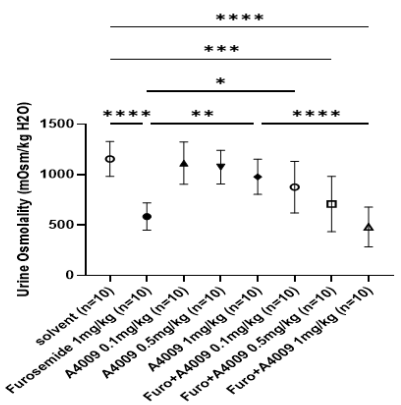

Figure 2. Effects of pendrin inhibition on urine output and electrolyte excretion in the wild type mice

(A) Urine output was significantly increased in the furosemide-treated group compared to the control group ($p < 0.0001$), confirming its diuretic effect. Co-administration of A4009 with furosemide further enhanced urine output as the dose increased, with furosemide + A4009 (0.5 mg/kg and 1 mg/kg) producing significantly elevated urine output compared to furosemide alone ($p < 0.0001$). Adding A4009 at 0.1 mg/kg and 0.5 mg/kg also led to a significant increase in urine output compared to furosemide alone ($p = 0.0003$, $p = 0.0023$), suggesting that pendrin inhibition independently contributes to urine output. (B, D) Sodium (Na^+) and chloride (Cl^-) excretion were significantly increased in the furosemide-treated group compared to the control ($p < 0.001$). Further enhancement of Na^+ and Cl^- excretion was observed in groups receiving both furosemide and A4009, reinforcing the role of pendrin in sodium-chloride balance. Furosemide + A4009 (1 mg/kg) treatment led to significantly higher sodium and chloride excretion compared to furosemide alone ($p = 0.0008$), and higher doses of A4009 (0.5 mg/kg and 1 mg/kg) further enhanced sodium excretion compared to lower doses ($p < 0.0001$). (C) Potassium (K^+) excretion remained unchanged with A4009 but was elevated in furosemide-treated groups. (E) Urine osmolality decreased significantly in the furosemide-treated group, and this effect was further enhanced in the furosemide + A4009 groups.

Statistical analysis was performed using one-way analysis of variance followed by Tukey's multiple comparisons test. Statistical significance was determined as follows: $*p < 0.05$; $** p < 0.01$; $*** p < 0.001$; $**** p < 0.0001$. All data are presented as mean ± SEM.

3.3 On-target specificity of pendrin inhibition in pendrin knockout mice

The on-target specificity of pendrin inhibition was evaluated using pendrin knockout mice (Figure 3). Western blot and qPCR analyses confirmed the absence of pendrin expression in the kidney, validating the KO model (Figure 3A,B). In this model, furosemide (1 mg/kg) significantly increased urine output compared to vehicle (adjusted $p < 0.0001$), indicating preserved responsiveness to loop diuretics. In contrast, A4009 monotherapy did not affect urine output ($p = 0.6066$), and co-administration with furosemide did not produce an additional effect beyond furosemide alone ($p = 0.1786$) (Figure 3C). Electrolyte analysis showed that furosemide significantly increased urinary sodium, chloride, and potassium excretion (all $p < 0.0001$), whereas A4009 had no significant effect in KO mice (Figure 3D–F). Similarly, urine osmolality was significantly reduced by furosemide, reflecting enhanced urine dilution, but remained unchanged with A4009 alone or in combination with furosemide in KO mice (Figure 3G). These findings indicate that the diuretic, natriuretic, and free urine output effects of A4009 are dependent on the presence of functional pendrin, supporting the on-target specificity of its action.

A

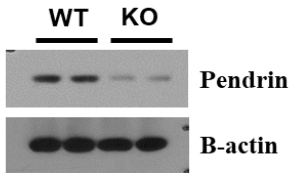

B

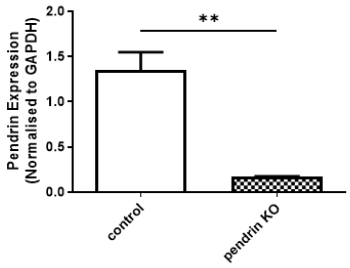

C

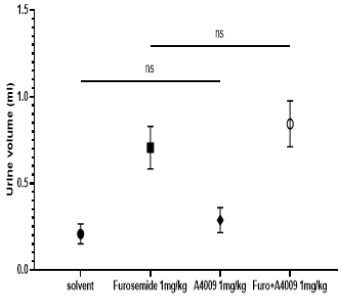

D

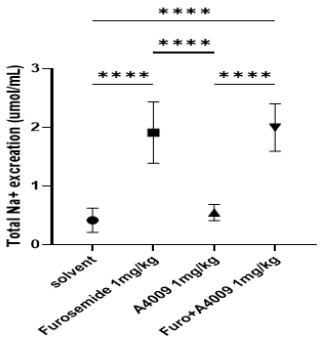

E

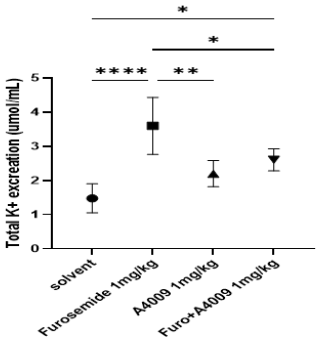

F

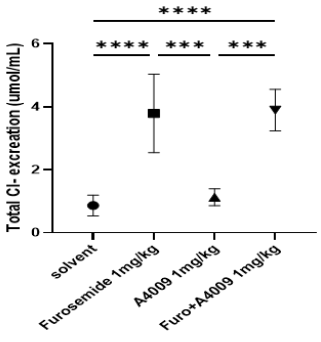

G

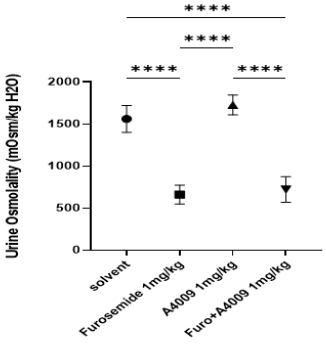

Figure 3. Effects of a pendrin inhibitor on urine Output and electrolyte excretion in pendrin knockout mice

(A–B) Western blot (A) and qPCR (B) analyses confirm the absence of pendrin expression in the kidneys of pendrin knockout mice, validating the model.

(C) In KO mice, furosemide (1 mg/kg) significantly increased urine output compared to vehicle, while A4009 alone had no effect. Co-treatment with A4009 and furosemide did not increase urine output beyond the effect of furosemide alone, indicating that A4009 does not promote diuresis in the absence of pendrin.

(D–F) Furosemide significantly increased urinary sodium, chloride, and potassium excretion, while A4009 had no significant effect in KO mice.

(G) Urine osmolality was significantly reduced by furosemide, consistent with increased urine dilution excretion. However, A4009 had no effect on osmolality, either alone or in combination with furosemide. These findings indicate that the effects of A4009 on urine output and electrolyte excretion depend on the presence of functional pendrin.

Statistical analysis was performed using one-way analysis of variance followed by Tukey's multiple comparisons test. Statistical significance was determined as follows: $*p < 0.05$; $** p < 0.01$; $*** p < 0.001$; $**** p < 0.0001$. All data are presented as mean ± SEM.

3.4 Diuretic efficacy of pendrin inhibitors was assessed in animal models with furosemide resistance model

The diuretic efficacy of a pendrin inhibitor was evaluated in an animal model with high-dose furosemide-induced diuretic resistance by measuring urine output and electrolyte excretion (Figure 4). Urine output was higher in the wild-type group, whereas the furosemide-resistant model showed a 37.6% reduction in urine output, suggesting that prolonged furosemide exposure impairs the furosemide response in urine production (Figure 4A). Furosemide (1 mg/kg) alone did not significantly increase urine output ($p = 0.7182$), confirming diuretic resistance. A4009 (1 mg/kg) modestly increased urine output ($p = 0.0446$), while lower doses had no effect compared to chronic furosemide infusion mice. Co-administration of furosemide and A4009 (0.5 mg/kg, 1 mg/kg) significantly enhanced urine output compared to both the solvent control ($p = 0.0003$, and $p < 0.0001$) and furosemide alone ($p < 0.0001$), indicating a synergistic effect of furosemide and A4009 (Figure 4B). Furosemide did not significantly increase sodium (Na^+) or chloride (Cl^-) excretion ($p = 0.1362$, $p = 0.1075$), consistent with diuretic resistance. A4009 (1 mg/kg) slightly increased sodium excretion ($p = 0.0340$), but lower doses did not increase in urinary sodium excretion. Furosemide + A4009 (0.5 mg/kg, 1 mg/kg) significantly enhanced sodium and chloride excretion compared to both the solvent control and furosemide alone ($p < 0.0001$), suggesting that pendrin inhibition restores sodium and chloride excretion in diuretic resistance model (Figure 4C, E). Furosemide and A4009 alone did not significantly affect potassium (K^+) excretion ($p = 0.6258$, p value). However, furosemide + A4009 (0.5 mg/kg, and 1 mg/kg) significantly increased urinary K^+ excretion ($p < 0.0001$), (Figure 4D). Urine osmolality was unchanged in the furosemide-treated group ($p = 0.5473$). However, furosemide + A4009 (0.5 mg/kg, 1 mg/kg) significantly reduced urine osmolality ($p < 0.0001$), suggesting that pendrin inhibition enhances urine dilution when combined with furosemide (Figure 4F). These findings demonstrate that pendrin inhibition enhances the diuretic response in a furosemide-resistant model by increasing urine output, restoring sodium and chloride excretion, and improving urine dilution ability.

A

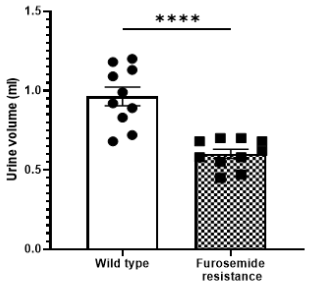

B

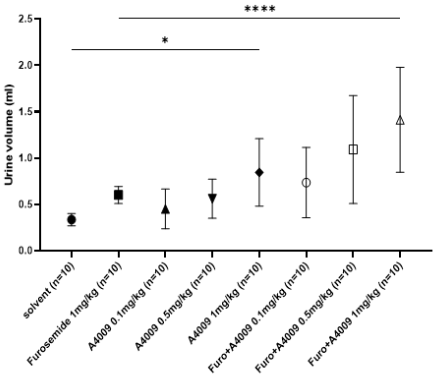

C

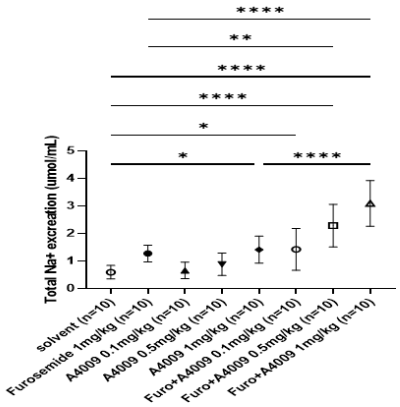

D

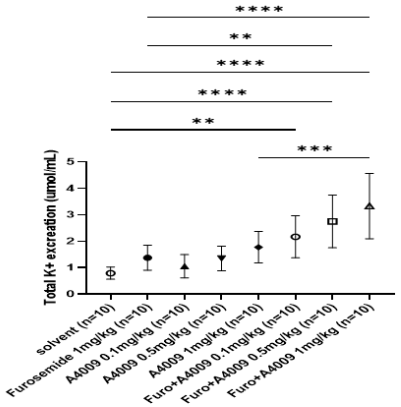

E

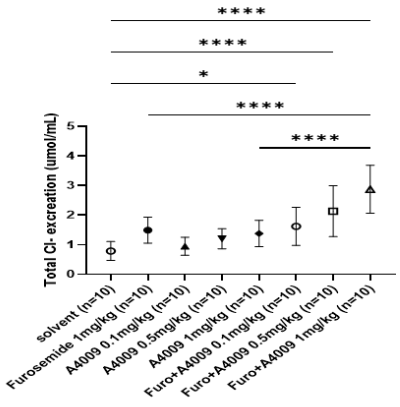

F

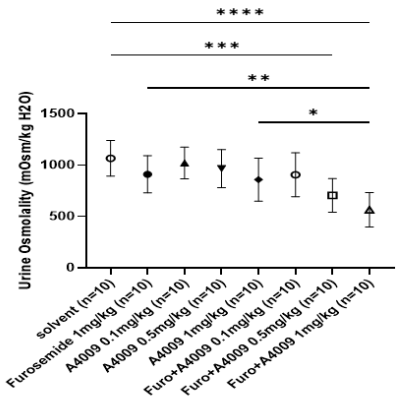

Figure 4. Effects of pendrin inhibition on urine output and electrolyte excretion in the furosemide resistant model

(A) Urine output was significantly higher in the wild-type group compared to the furosemide-resistant model. Following high-dose furosemide treatment, diuretic resistance was induced, resulting in a 37.6% reduction in urine output. This suggests that prolonged furosemide exposure diminishes diuretic efficacy. (B) Urine output was significantly increased by A4009 (1 mg/kg) compared to the control ($p = 0.0446$), indicating a modest diuretic effect in the chronic furosemide infusion model. When A4009 was co-administered with furosemide, urine output was further elevated as the A4009 dose increased, with furosemide + A4009 (0.5 mg/kg and 1 mg/kg) resulting in significantly higher urine output than furosemide alone ($p = 0.0003$, $p < 0.0001$). (C, E) Sodium (Na^+) and chloride (Cl^-) excretion in urine were significantly increased in the furosemide + A4009 groups compared to the solvent control ($p < 0.0001$). Co-administration of A4009 and furosemide further enhanced sodium and chloride excretion compared to furosemide alone ($p < 0.0001$). (D) Potassium (K^+) excretion remained unchanged with A4009 alone but was significantly increased in the furosemide + A4009 (furo+A4009 0.1 mg, 0.5 mg and 1 mg/kg) groups compared to the control ($p = 0.0015$, $p < 0.0001$), suggesting that pendrin inhibition contributes to increased potassium excretion when combined with furosemide. Urine osmolality was significantly reduced in the furosemide-treated groups compared to the control ($p < 0.0001$), and this effect was further enhanced with A4009 co-administration as the dose increased ($p < 0.0001$).

Statistical analysis was performed using one-way analysis of variance followed by Tukey's multiple comparisons test. Statistical significance was determined as follows: *$p < 0.05$; ** $p < 0.01$; *** $p < 0.001$; **** $p < 0.0001$. All data are presented as mean ± SEM.

3.5 Diuretic efficacy of a pendrin inhibitor was assessed in angiotensin II-induced hypertensive models

Urine output and electrolyte excretion were assessed to evaluate the diuretic efficacy of pendrin inhibition in an angiotensin II-induced model (Figure 5). Furosemide (1 mg/kg) alone did not significantly increase urine output ($p = 0.0916$), indicating reduced diuretic responsiveness in this model. A4009 (0.1–1 mg/kg) alone had no effect ($p > 0.05$), but co-administration with furosemide (0.5–1 mg/kg) significantly increased urine output compared to both the solvent control ($p < 0.0001$) and furosemide alone ($p = 0.001$), (Figure 5A). Furosemide significantly increased sodium (Na^+) excretion ($p = 0.0121$), while A4009 alone had no significant effect ($p > 0.05$). A4009 (1 mg/kg) induced a modest increase ($p = 0.0199$), and when combined with furosemide (0.5–1 mg/kg), sodium excretion was further enhanced ($p < 0.0001$), indicating a synergistic effect of pendrin inhibition (Figure 5B, D). Chloride (Cl^-) excretion followed a similar pattern, with furosemide alone significantly increasing Cl^- excretion ($p = 0.0007$), while A4009 alone had no effect. However, furosemide + A4009 (0.5–1 mg/kg) significantly increased Cl^- excretion as the dose increased ($p < 0.0001$), suggesting restored chloride excretion under hypertensive conditions. Furosemide did not significantly alter potassium (K^+) excretion ($p = 0.1362$), but A4009 (1 mg/kg) alone increased K^+ excretion ($p = 0.0038$). Co-administration with furosemide (0.5–1 mg/kg) further elevated K^+ excretion ($p < 0.0001$), suggesting pendrin inhibition enhances furosemide-induced potassium excretion (Figure 5C). Urine osmolality decreased significantly with furosemide ($p < 0.0001$), confirming increased free water clearance. A4009 alone had no effect, but its combination with furosemide (0.5–1 mg/kg) further reduced urine osmolality ($p < 0.0001$), indicating enhanced free water clearance through pendrin inhibition (Figure 5E). These findings suggest that pendrin inhibition amplifies the diuretic effects of furosemide in angiotensin II-induced model by increasing urine output, enhancing sodium and chloride excretion, and improving free water clearance. The dose-dependent potentiation of furosemide's effects highlights the potential of pendrin inhibitors as a therapeutic strategy to enhance diuretic response in hypertension.

A

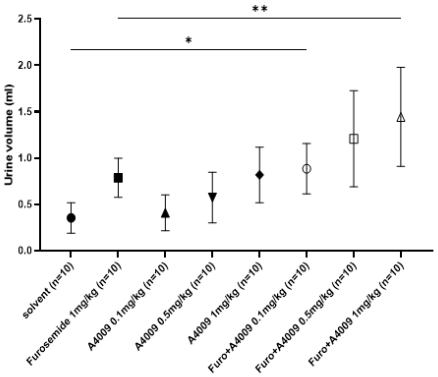

B

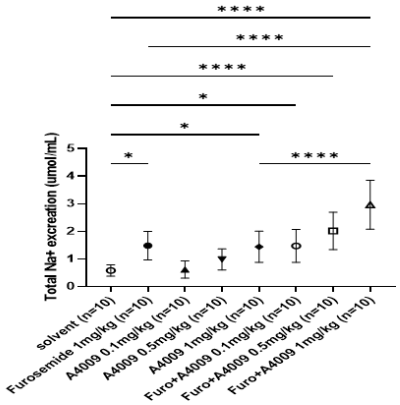

C

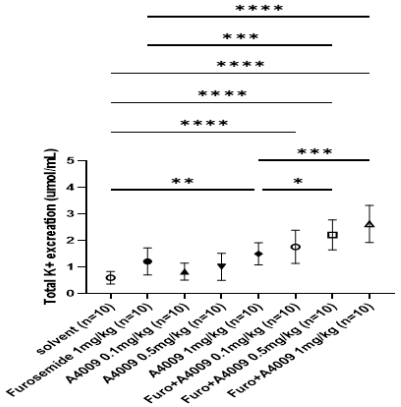

D

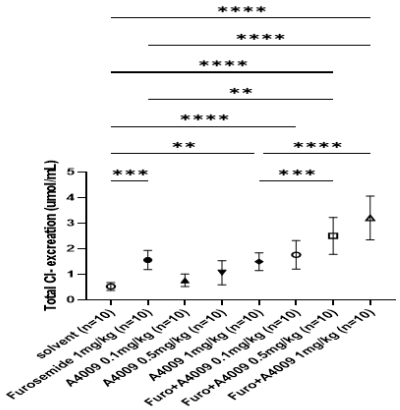

E

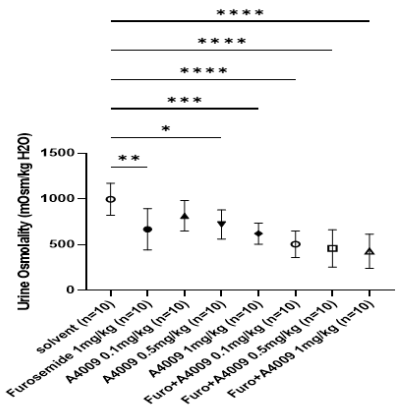

Figure 5. Effects of pendrin inhibition on urine output and electrolyte excretion in angiotensin II-induced hypertensive models

(A) Urine output was modestly higher in the A4009 (1 mg/kg) group compared to the solvent control ($p = 0.0916$), suggesting a mild diuretic effect. Co-administration of A4009 with furosemide (0.5 mg/kg, 1 mg/kg) further increased urine output as the dose of A4009 increased, with significant differences compared to both the solvent control ($p = 0.0157$, $p < 0.0001$) and furosemide alone ($p = 0.0010$). These findings indicate that pendrin inhibition enhances the diuretic response to furosemide in the angiotensin II-induced model.

(B, D) Sodium (Na^+) and chloride (Cl^-) excretion were significantly increased in the furosemide + A4009 (0.5 mg/kg, 1 mg/kg) groups compared to the solvent control ($p < 0.0001$). Moreover, co-administration of A4009 with furosemide further elevated Na^+ and Cl^- excretion relative to furosemide alone ($p < 0.0001$), highlighting a synergistic effect of pendrin inhibition on sodium and chloride handling under hypertensive conditions.

(C) Potassium (K^+) excretion remained unchanged with A4009 alone but was significantly increased in the furosemide + A4009 (0.5 mg/kg, 1 mg/kg) groups compared to the solvent control ($p < 0.0001$), indicating that pendrin inhibition contributes to enhanced K^+ excretion when combined with furosemide.

(E) Urine osmolality was significantly reduced in the furosemide-treated groups compared to the solvent control ($p < 0.0001$), and this reduction was further intensified with A4009 co-administration as the dose increased ($p < 0.0001$), suggesting improved urine dilution when pendrin inhibition is combined with furosemide.

Statistical analysis was performed using one-way analysis of variance followed by Tukey's multiple comparisons test. Statistical significance was determined as follows: *$p < 0.05$; ** $p < 0.01$; *** $p < 0.001$; **** $p < 0.0001$. All data are presented as mean ± SEM.

3.6 Redistribution of tubular transporters in Furosemide resistance model

Immunofluorescence analysis was conducted to examine the expression and localization of key sodium transporters in the kidneys of mice with high-dose furosemide-induced diuretic resistance (Figure 6). Pendrin expression was significantly upregulated in the collecting ducts of the furosemide-treated group, with enhanced fluorescence intensity along the apical membrane. This suggests a compensatory mechanism for sodium reabsorption in response to chronic furosemide exposure (Figure 6A). NKCC2 expression in the thick ascending limb of Henle's loop remained unchanged despite prolonged furosemide treatment (Figure 6B). NCC expression in the distal convoluted tubule (DCT) was markedly increased following furosemide administration, with a shift to the apical membrane. (Figure 6C). ENaCα expression in the collecting duct was significantly elevated, particularly along the apical membrane of principal cells. (Figure 6D).

A

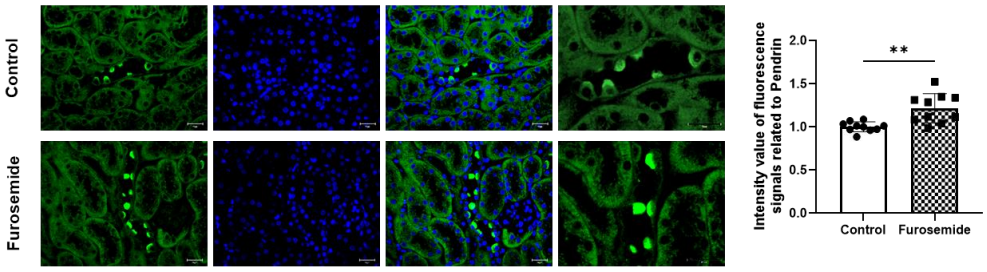

B

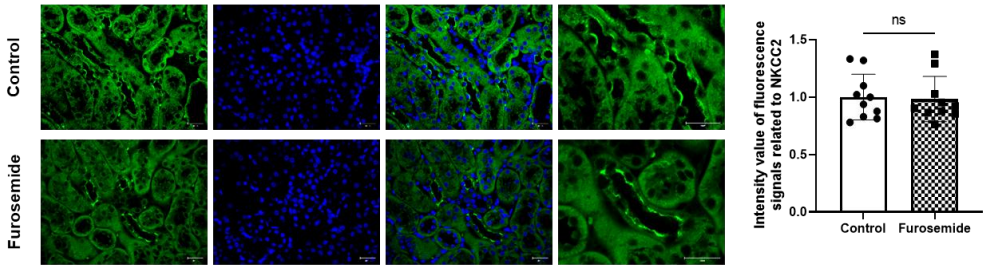

C

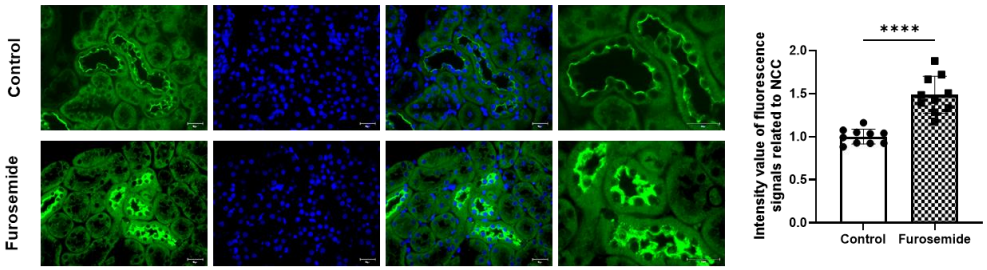

D

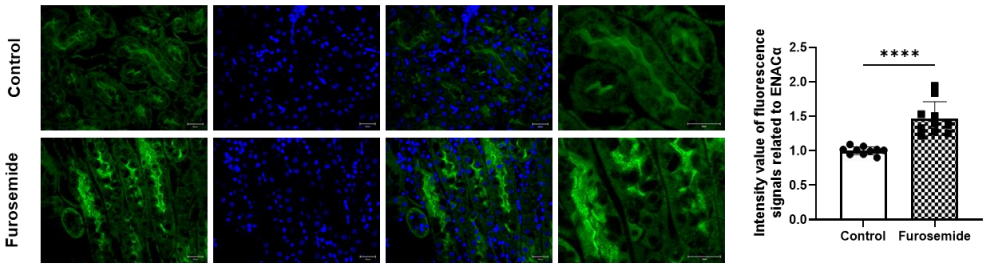

Figure 6. Immunofluorescence analysis of sodium transporter expression and localization in furosemide resistant model.

immunofluorescence images show the localization of (A) Pendrin, (B) NKCC2, (C) NCC, and (D) ENaCα (green) in kidney sections from control and furosemide-treated groups. Nuclei were counterstained with DAPI (blue). White arrows indicate regions with increased apical localization in response to furosemide treatment. (A) Pendrin expression in the collecting ducts was significantly increased in the furosemide-treated group, with enhanced fluorescence intensity along the apical membrane,. (B) NKCC2 expression in the thick ascending limb of Henle's loop remained unchanged, indicating that NKCC2 levels are maintained despite chronic furosemide administration. (C) NCC expression in the distal convoluted tubule (DCT) was markedly increased following furosemide treatment,. (D) ENaCα expression in the collecting duct was significantly elevated, with strong apical membrane localization in principal cells,.

Images were acquired at 40X magnification, and scale bars represent 50 μm. The right panels show quantification of fluorescence intensity for each transporter.

Statistical analysis was performed using Two-tailed unpaired Student's t-test, with statistical significance determined as follows: *$p < 0.05$; ** $p < 0.01$; *** $p < 0.001$; **** $p < 0.0001$. All data are presented as mean ± SEM.

3.7 Protein and mRNA expression of Sodium transporter in furosemide resistance model

Western blot and RT-qPCR analyses were performed to change in sodium transporters in a high-dose furosemide-induced resistance model (Figure 7). Protein expression analysis revealed a significant increase in pendrin, NCC, and ENaC in the furosemide-treated group compared to controls (Figure 7A, B, C, E). In contrast, NKCC2 expression remained unchanged, suggesting that adaptive mechanisms underlying furosemide resistance primarily occur in the distal nephron rather than in the thick ascending limb (TAL) of the loop of Henle (Figure 7A, D). Additionally, AGTR1 and Rac1 expression levels were significantly elevated, indicating RAAS pathway and Rac1 activation in response to chronic diuretic exposure (Figure 7A, F, G). To determine whether these changes were transcriptionally regulated, RT-qPCR analysis was conducted. Consistent with the protein expression data, mRNA levels of pendrin, NCC, ENaC, and Rac1 were significantly increased in the furosemide-treated group, whereas NKCC2 mRNA expression remained unchanged (Figure 7H–L). These findings suggest that increased AGTR1 and Rac1 expression supports the involvement of RAAS activation in sodium transporter regulation, potentially contributing to sodium retention and reduced diuretic efficacy of furosemide.

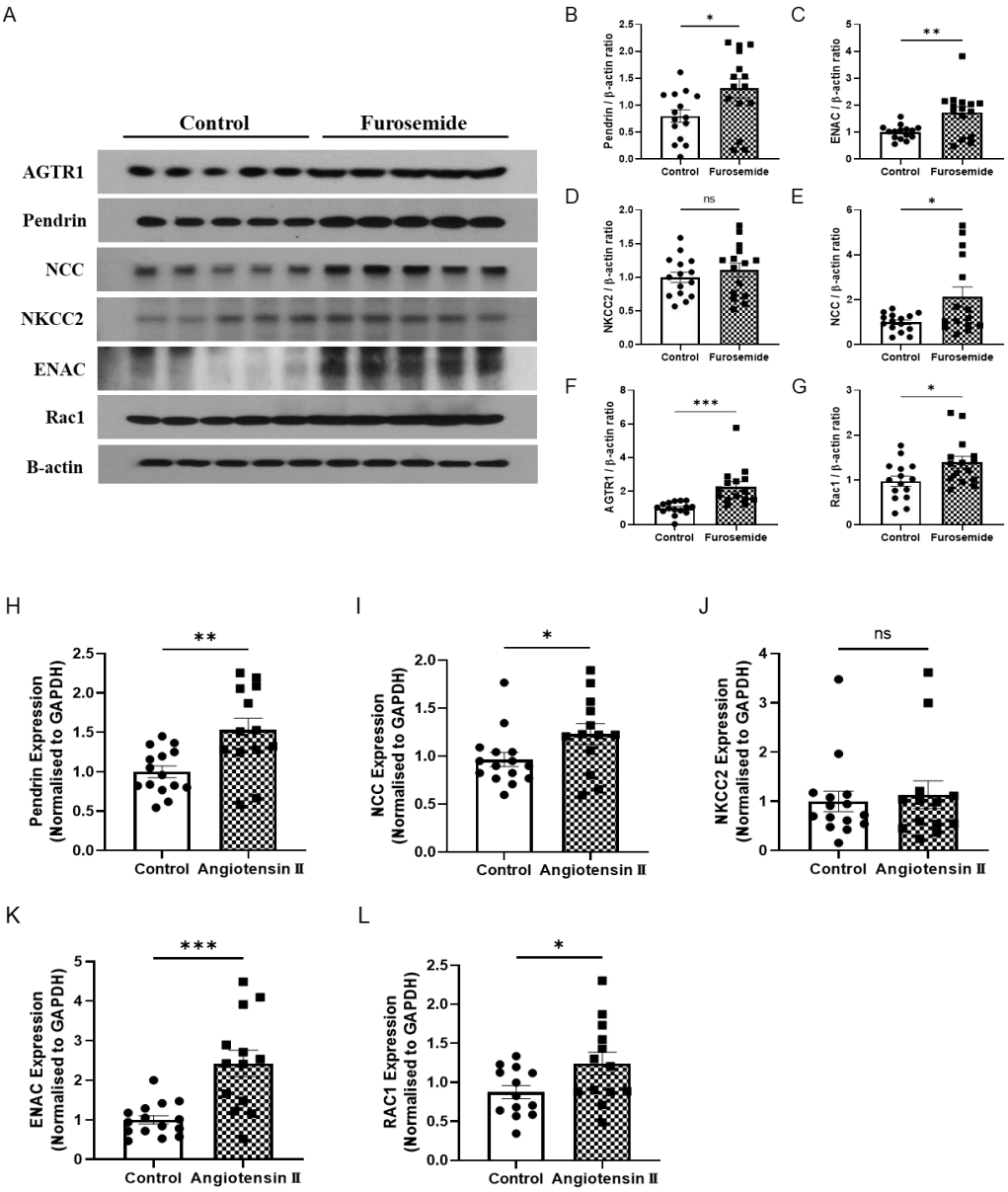

Figure 7. Protein and mRNA expression of sodium transporters in Furosemide resistance model

(A-G) Protein expression levels of sodium transporters and RAAS-related proteins in a high-dose furosemide-induced resistance model. Western blot analysis showed a significant increase in pendrin, NCC, ENaC, AGTR1, and Rac1 expression in furosemide-treated mice compared to controls, whereas NKCC2 expression remained unchanged. (H-L) mRNA expression levels of sodium transporters and RAAS-related proteins. The mRNA expressions of pendrin, NCC, ENaC, and Rac1 were significantly increased in furosemide-treated mice compared to controls, while NKCC2 expression showed no significant difference.

Statistical analysis was performed using one-way analysis of variance ollowed by Tukey's multiple comparisons test. Statistical significance was determined as follows: *$p < 0.05$; ** $p < 0.01$; *** $p < 0.001$; **** $p < 0.0001$. All data are presented as mean ± SEM.

3.8 Volcano plot of differentially expressed genes (DEGs) in furosemide treatment model

The volcano plot analysis reveals significant transcriptional changes in response to high-dose furosemide-induced diuretic resistance model, highlighting key compensatory mechanisms in renal sodium handling. Slc26a4 (Pendrin), Scnn1a, Scnn1g (ENaC subunits), and Slc12a3 (NCC) were significantly upregulated. Concurrently, Rac1 (Rac Family Small GTPase 1), Nr3c2 (mineralocorticoid receptor, MR) and Cyp11b2 (aldosterone synthase) were elevated, indicating increased aldosterone signaling, while Agtr1a and Ace were downregulated, possibly reflecting feedback inhibition of the renin-angiotensin system. In contrast, Scnn1b (ENaC β-subunit) and Nedd4, a key regulator of ENaC degradation, were significantly downregulated, further supporting a shift toward enhanced sodium retention. These findings suggest that furosemide-induced sodium depletion triggers a robust compensatory response involving Pendrin, ENaC, and aldosterone pathways, contributing to diuretic resistance.

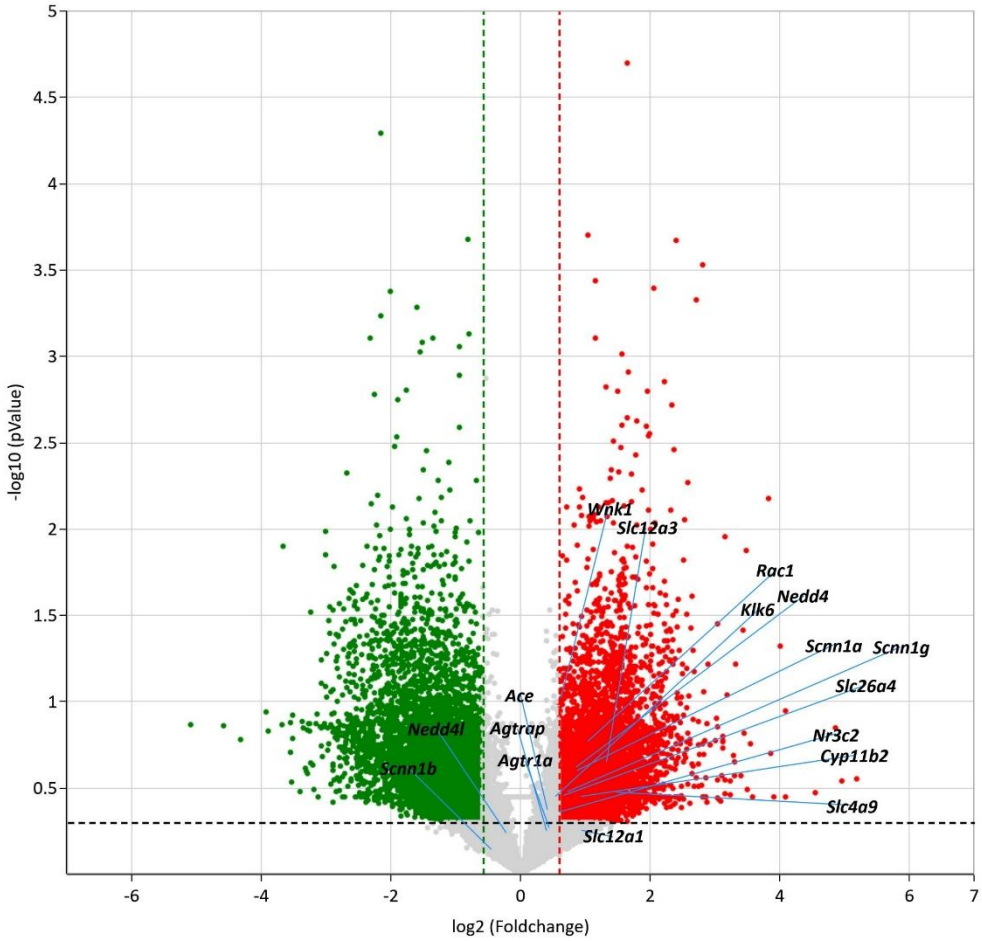

Figure 8. Volcano plot of differentially expressed genes (DEGs)

The volcano plot (Figure 14). illustrates the differentially expressed genes, with upregulated genes (red) and downregulated genes (green) following furosemide resistance model (n=4 per group). Notably, Slc26a4 and Scnn1b were among the most significantly upregulated genes, consistent with a potential compensatory response to maintain sodium homeostasis. The X-axis represents gene expression changes (log_2-Fold Change), while the Y-axis represents statistical significance (-log_{10}-value).

3.9 Protein-protein interaction in the furosemide resistance model

Protein-protein interaction (PPI) analysis revealed a strong functional association between Rac1, Slc26a4 (Pendrin), and sodium transport–related genes, including Slc12a3 (NCC) and Scnn1a, Scnn1b, Scnn1g (ENaC subunits) (Figure 9). In this network, Rac1 was functionally linked to several regulators of sodium homeostasis, supporting the hypothesis that Rac1-mediated Pendrin upregulation contributes to sodium retention in response to chronic diuretic exposure.

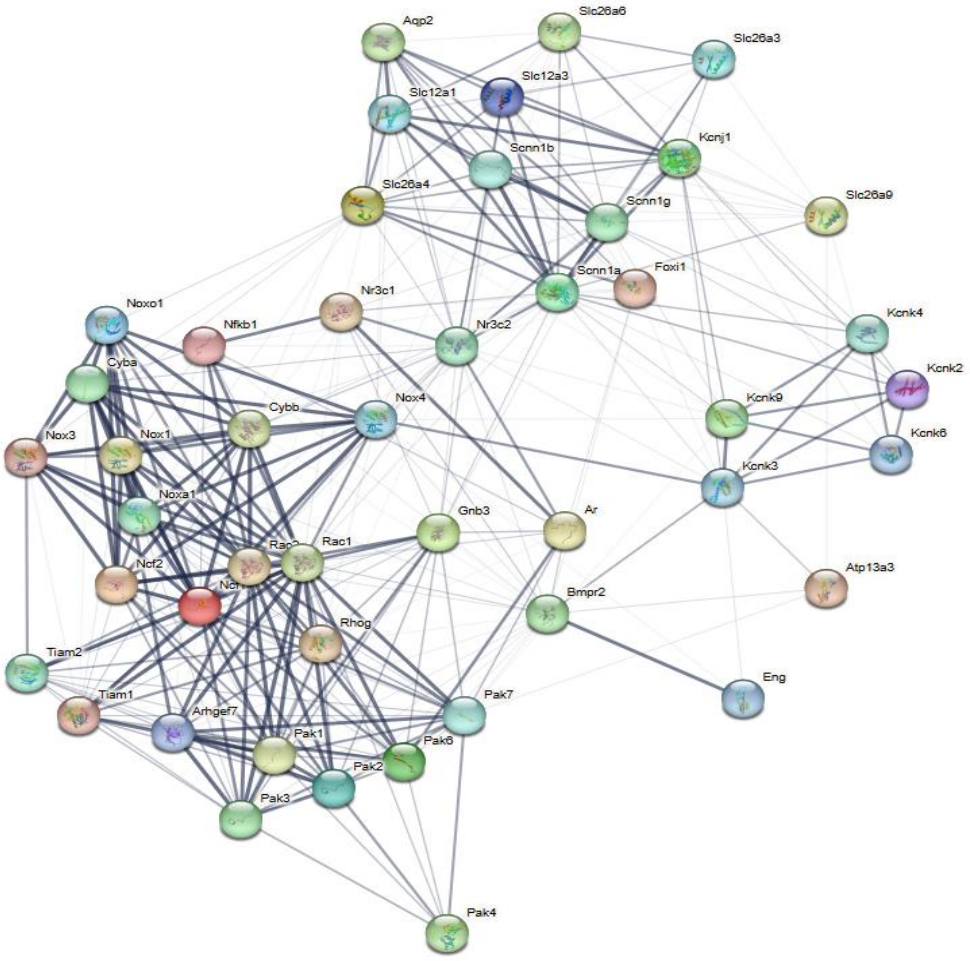

Figure 9. Protein-protein interaction (PPI) network analysis

This Protein-Protein Interaction (PPI) network was constructed to explore the molecular interactions between differentially expressed proteins in response to furosemide treatment (n=4 per group). The network reveals functional relationships among key transporters, signaling molecules, and regulatory proteins involved in renal ion transport and diuretic resistance mechanisms.

3.10 Angiotensin II-mediated sodium transporter redistribution

Immunofluorescence analysis was performed to assess the expression and subcellular localization of sodium transporters in the kidneys of angiotensin II-indused mice (Figure 10). Pendrin (SLC26A4) expression was significantly upregulated in the collecting ducts of angiotensin II-induced mice, with a marked increase in fluorescence intensity along the apical membrane of type B and non-A, non-B intercalated cells. This suggests that angiotensin II enhances Pendrin expression and its apical localization, facilitating chloride-bicarbonate exchange and contributing to sodium retention (Figure 10A). NKCC2 expression in the thick ascending limb of Henle's loop showed no significant difference between control and angiotensin II-induced mice. (Figure 10B). NCC expression in the distal convoluted tubule (DCT) was significantly increased following angiotensin II-induced model, with redistribution from the cytoplasm to the apical membrane. (Figure 10C). ENaCα expression in the collecting duct was significantly upregulated, with increased fluorescence intensity along the apical membrane of principal cells. (Figure 10D). In addition to changes in transporter expression, subcellular redistribution was observed in angiotensin II-indused model kidneys.

A

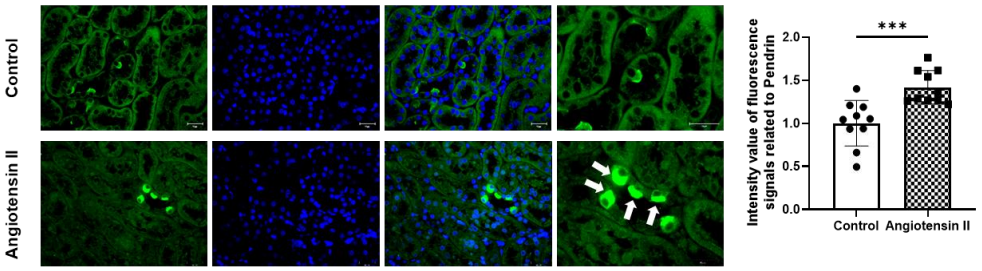

B

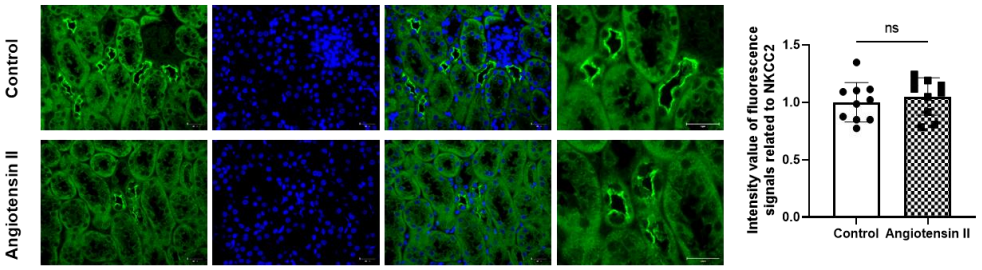

C

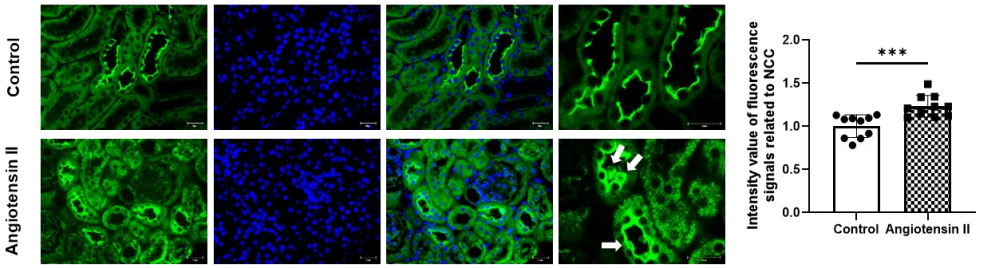

D

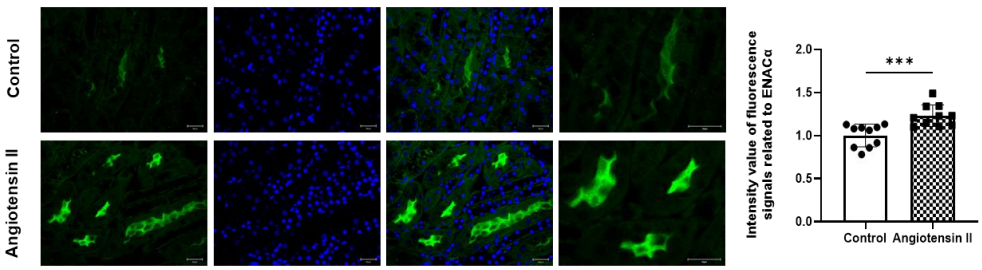

Figure 10. Immunofluorescence analysis of sodium transporter expression and localization in the angiotensin II-induced model.

Immunofluorescence images show the localization of (A) Pendrin, (B) NKCC2, (C) NCC, and (D) ENaCα (green) in kidney sections from control and angiotensin II-induced groups. Nuclei are counterstained with DAPI (blue). White arrows indicate regions with increased apical localization in response to angiotensin II-induced model. (A) Pendrin expression in the collecting ducts was significantly increased in the angiotensin II-induced group, with enhanced fluorescence intensity along the apical membrane of type B and non-A, non-B intercalated cells. (B) NKCC2 expression in the thick ascending limb of Henle's loop remained unchanged,. (C) NCC expression in the distal convoluted tubule (DCT) was markedly increased following angiotensin II-induced model, accompanied by a shift from the cytoplasm to the apical membrane. (D) ENaCα expression in the collecting duct was significantly elevated, with strong apical membrane localization in principal cells.

Images were acquired at 40X magnification, and scale bars represent 50 μm. The right panels show quantification of fluorescence intensity for each transporter.

Statistical analysis was performed using Two-tailed unpaired Student's t-test. Statistical significance was determined as follows: $*p < 0.05$; $** p < 0.01$; $*** p < 0.001$; $**** p < 0.0001$. All data are presented as mean ± SEM.

3.11 Protein and mRNA expression of sodium transporter in angiotensin II-induced hypertension model

Western blot and RT-qPCR analyses were performed to investigate the molecular mechanisms underlying sodium transporter upregulation in an angiotensin II-induced model (Figure 11). Protein expression analysis revealed a significant increase in pendrin (SLC26A4), NCC (SLC12A3), and ENaC (SCNN1α) in the angiotensin II-induced group compared to controls (Figure 11A, B, C, E). In contrast, NKCC2 (SLC12A1) expression remained unchanged (Figure 11A, D). Additionally, AGTR1 and Rac1 expression levels were significantly elevated, indicating RAAS pathway activation in response to angiotensin II stimulation (Figure 11A, F, G). To determine whether these changes were transcriptionally regulated, RT-qPCR analysis was performed. Consistent with the protein expression data, pendrin, NCC, ENaC, and Rac1 mRNA levels were significantly increased in the angiotensin II-induced group, whereas NKCC2 mRNA expression remained unchanged (Figure 11H–L). Furthermore, the increased expression of AGTR1 and Rac1 supports the role of RAAS activation in sodium transporter regulation, which may contribute to sodium retention and the hypertensive effects of angiotensin II.

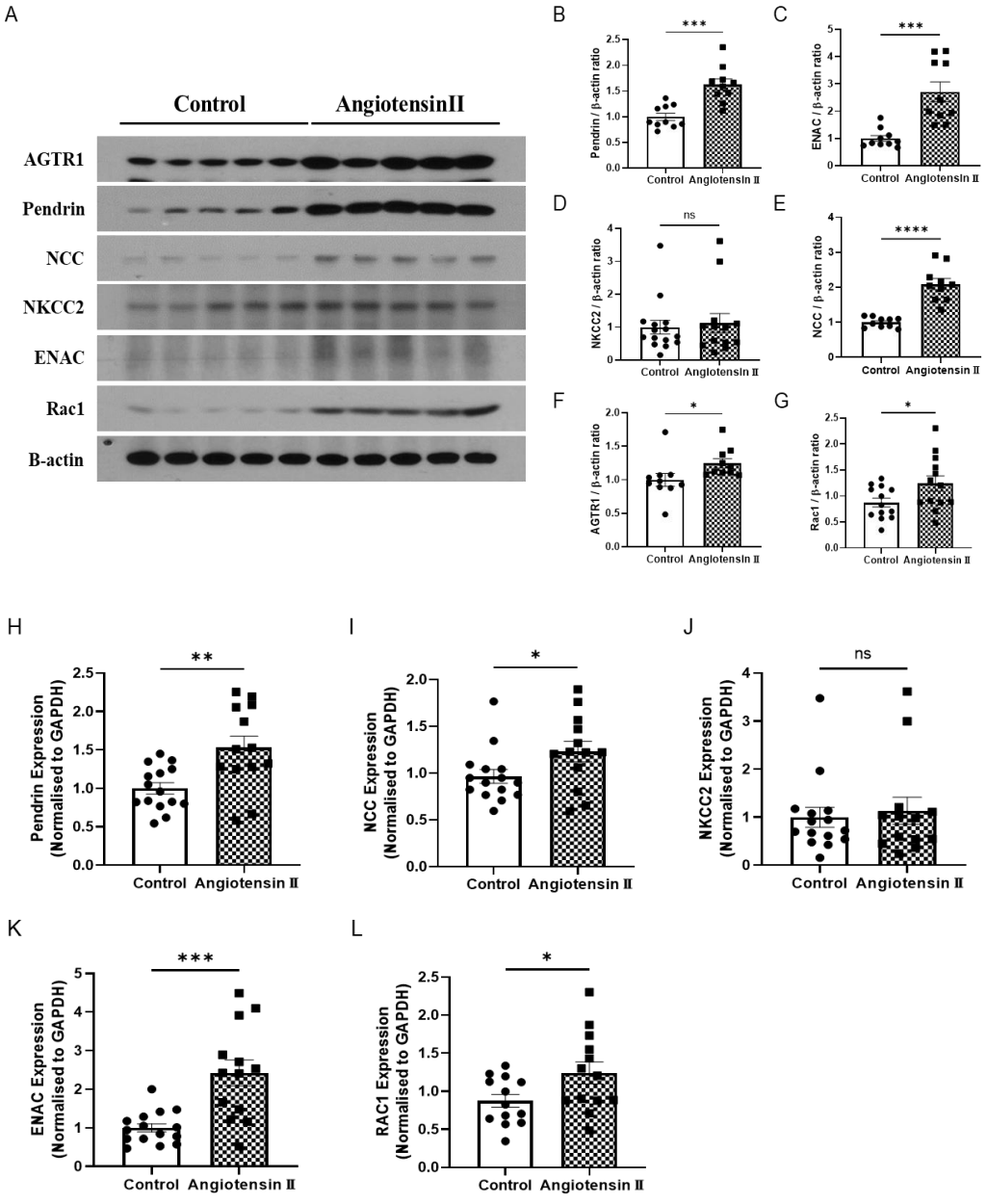

Figure 11. Protein and mRNA expression of sodium transporter in angiotensin II-induced hypertension model

(A–G) Protein expression levels of sodium transporters and RAAS-related proteins in an angiotensin II-induced model. Western blot analysis revealed a significant increase in pendrin (SLC26A4), NCC (SLC12A3), ENaC (SCNN1α), AGTR1, and Rac1 expression in angiotensin II-induced mice compared to controls, whereas NKCC2 (SLC12A1) expression remained unchanged. (H–L) mRNA expression levels of sodium transporters and RAAS-related proteins. RT-qPCR analysis showed that pendrin, NCC, ENaC, and Rac1 mRNA levels were significantly increased in angiotensin II-induced mice compared to controls, while NKCC2 mRNA expression showed no significant difference.

Statistical analysis was performed using one-way analysis of variance followed by Tukey's multiple comparisons test. Statistical significance was determined as follows: *$p < 0.05$; ** $p < 0.01$; *** $p < 0.001$; **** $p < 0.0001$. All data are presented as mean ± SEM.

3.12 Pendrin inhibition reduces on blood pressure in angiotensin II-induced hypertension model

Systolic and diastolic blood pressure were measured to evaluate the effect of pendrin inhibition in an angiotensin II-induced hypertensive model. Angiotensin II treatment resulted in a significant increase in systolic blood pressure compared to the control group. Administration of A4009 in the angiotensin II group attenuated the increase in systolic blood pressure, whereas A4009 treatment had no significant effect on blood pressure in normotensive controls (Figure 12).

These findings suggest that pendrin inhibition selectively lowers blood pressure in hypertensive conditions, potentially by reducing sodium retention.

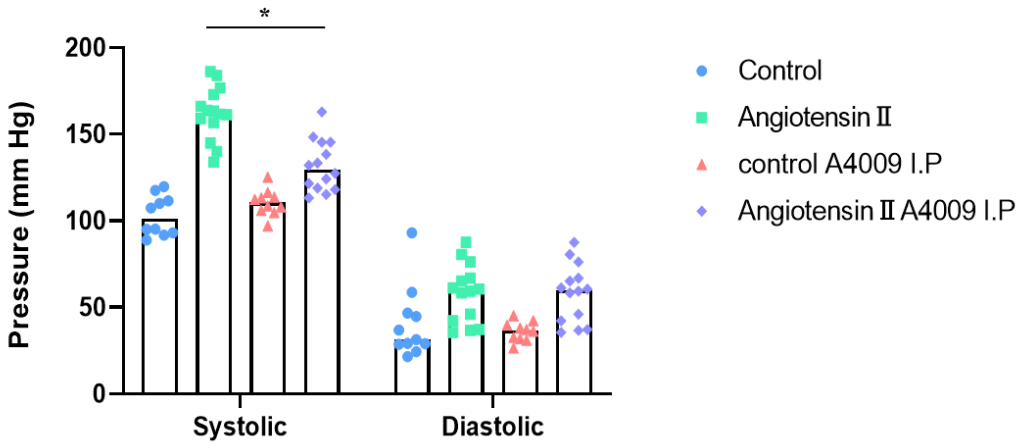

Figure 12. Effect of pendrin inhibition on blood pressure in angiotensin II-induced hypertension model

Blood pressure measurements were conducted to evaluate the effect of pendrin inhibition in an angiotensin II-induced model. Systolic blood pressure was significantly increased in the angiotensin II-induced group compared to the control group,. However, administration of A4009 resulted in a significant reduction in systolic blood pressure in the angiotensin II-induced hypertension group,. No significant changes were observed in diastolic blood pressure across groups.

statistical analysis was performed using two-way analysis of variance with Tukey's multiple comparisons and two-tailed unpaired student's t-test: *$p < 0.05$; ** $p < 0.01$; *** $p < 0.001$; **** $p < 0.0001$. All data are presented as mean ± SEM.

3.13 Regulation of Pendrin, Rac1, and NR3C2 mRNA by Aldosterone and Angiotensin II: Involvement of Rac1 and NR3C2 Signaling

Pendrin mRNA expression was significantly upregulated following treatment with aldosterone and angiotensin II (Figure 13). Co-treatment with angiotensin II and either the Rac1 inhibitor NSC23766 or the MR antagonist spironolactone significantly reduced pendrin mRNA expression(Figure 13A). Similarly, Rac1 mRNA expression was increased by aldosterone and angiotensin II stimulation and was significantly decreased by NSC23766 or spironolactone treatment (Figure 13B). In addition, NR3C2 mRNA expression was significantly upregulated by angiotensin II and was attenuated by co-treatment with either NSC23766 or spironolactone(Figure 13C). These results indicate that aldosterone and angiotensin II increase the mRNA expression of pendrin and Rac1, and that angiotensin II also induces NR3C2 expression. Furthermore, both Rac1 inhibition and MR antagonism suppress the upregulation of pendrin, Rac1, and NR3C2 mRNA expression.

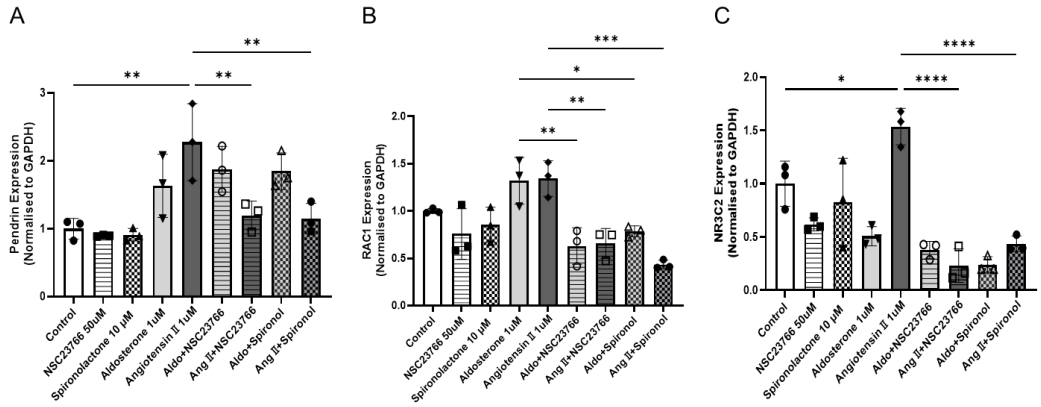

Figure 13. mRNA expression levels of pendrin,Rac1 and NR3C2 in mouse collecting duct cells under treatment conditions

qPCR analysis was performed to evaluate the mRNA expression of pendrin and Rac1 in mouse collecting duct cells following treatment with NSC23766 (50 μM, Rac1 inhibitor), spironolactone (10 μM), aldosterone (1 μM), and angiotensin II (1 μM).

(A) Pendrin mRNA expression was significantly upregulated following aldosterone and angiotensin II treatment. NSC23766 treatment significantly reduced pendrin expression in the aldosterone and angiotensin II-treated groups. (B) Rac1 mRNA expression was also upregulated in response to aldosterone and angiotensin II. NSC23766 treatment significantly reduced Rac1 expression. (C) NR3C2 mRNA expression was significantly increased by angiotensin II treatment. Co-treatment with NSC23766 or spironolactone significantly attenuated this angiotensin II-induced upregulation.

Statistical analysis was performed using one-way analysis of variance ollowed by Tukey's multiple comparisons test. Statistical significance was determined as follows: *$p < 0.05$; ** $p < 0.01$; *** $p < 0.001$; **** $p < 0.0001$. All data are presented as mean ± SEM.

3.14. Pendrin-Rac1 interaction in collecting duct cells is enhanced by angiotensin II and aldosterone

A Proximity ligation assay (PLA) was performed to evaluate the interaction between pendrin and Rac1 in mouse collecting duct cells. (Figure 14). Under control conditions, minimal pendrin-Rac1 interactions were observed, suggesting a low basal interaction. However, aldosterone and angiotensin II treatment significantly increased pendrin-Rac1 interactions. In both aldosterone and angiotensinII treated groups, Rac1 inhibition significantly reduced pendrin-Rac1 interactions. This finding suggest that Rac1 acts as a key mediator in the upregulation and activation of pendrin induced by aldosterone and angiotensin II.

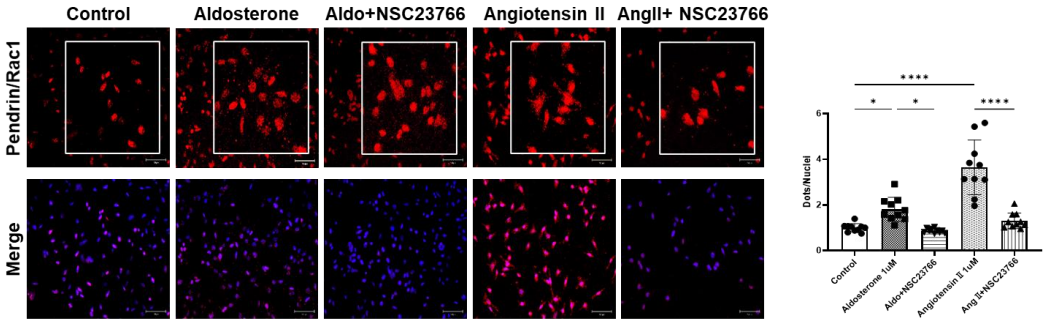

Figure 14. Proximity ligation assay (PLA) analysis of pendrin-Rac1 interaction in mouse collecting duct cells

PLA images showing pendrin-Rac1 interactions (red) in control, aldosterone-treated, aldosterone + NSC23766-treated, angiotensin II-treated, and angiotensin II + NSC23766-treated cells. Nuclei were stained with DAPI (blue). Aldosterone and angiotensin II treatment significantly increased pendrin-Rac1 interactions. Treatment with the Rac1 inhibitor NSC23766 significantly reduced these interactions in both aldosterone and angiotensin II-treated groups.

Images were acquired at 20× magnification, and the scale bar represents 150 μm.

Statistical analysis was performed using two-way analysis of variance with Tukey's multiple comparisons and two-tailed unpaired Student's t-test. Statistical significance is indicated as follows: *$p < 0.05$; ** $p < 0.01$; *** $p < 0.001$; **** $p < 0.0001$. All data are presented as mean ± SEM.

4. DISCUSSION

This study demonstrates that A4009, a novel pendrin inhibitor, exerts significant diuretic effects in mouse models of chronic furosemide administration and angiotensin II infusion. The combination of A4009 with furosemide was also associated with an additive effect in the diuretic resistance model. Treatment with A4009 significantly reduced blood pressure in the angiotensin II-induced hypertension model, suggesting its potential as an antihypertensive agent in RAAS-driven conditions.

Diuretic resistance remains a significant clinical challenge in the management of patients with chronic kidney disease (CKD) and heart failure, where escalating doses of loop diuretics fail to induce adequate natriuresis and fluid removal. Prolonged diuretic use, especially loop diuretics leads to compensatory sodium resorption in different nephron segments. Loop diuretics block Na^+-K^+-$2Cl^-$ transporters in the thick ascending limb, however, sodium reabsorption increases in the distal convoluted tubule and collecting duct. Hoorn and Ellison have emphasized that diuretic resistance arises from several mechanisms, including post-diuretic sodium retention, within-dose tolerance, and enhanced sodium reabsorption in distal nephron segments[23].

Present study demonstrated that chronic administration of furosemide led to increased expression of NCC, pendrin and ENaC, which likely contributed to the blunted diuretic response to furosemide. These findings are consistent with previous studies indicating that long-term loop diuretic treatment induces structural and molecular remodeling of the distal nephron, including upregulation of sodium transport proteins such as NCC, ENaC, and pendrin[24, 25]. In wild type mice, the administration of a pendrin inhibitor alone did not produce a significant diuretic effect. However, in a model of chronic furosemide treatment, a high dose of the pendrin inhibitor led to an enhanced diuretic effect. This finding suggests that the diuretic effect of A4009 is more pronounced in a diuretic resistance model, where pendrin expression is upregulated.

In addition, furosemide-induced hypovolemia and reduced renal perfusion are known to activate the RAAS, which enhances pendrin expression in the collecting duct, thereby increasing sodium reabsorption and attenuating diuretic efficacy. Angiotensin II activates WNK-SPAK/OSR1 signaling, which enhances the expression and membrane localization of several sodium transporters, including NCC and ENaC[26]. Moreover, angiotensin II and aldosterone are well-known stimulators of pendrin activation. Angiotensin itself, as well as aldosterone upregulated by angiotensin II, enhances pendrin activity. Consistent with previous findings, my data demonstrated increased expression of pendrin and ENaC in the angiotensin II-induced model. The angiotensin II-induced mice showed also blunted

diuretic response to furosemide, whereas treatment with A4009 or its combination with furosemide potentiated the diuretic effect in this model[27].

Since adaptive increases in Na^+ reabsorption in the distal convoluted tubules and collecting ducts offset the effects of loop diuretics, thiazide-like diuretics or aldosterone antagonists are often combined with loop diuretics to overcome diuretic resistance. However, thiazide diuretics are associated with adverse side effects, such as hyponatraemia, hypokalaemia, and acute kidney injury. In addition, aldosterone antagonists can exacerbate hyperkalemia, a condition commonly observed in patients with heart failure and chronic kidney disease (CKD) who also exhibit diuretic resistance. In this study, I found that A4009 effectively enhances the diuretic response when combined with furosemide in both chronic furosemide-treated and angiotensin II-induced models. Cil et al. have suggested that pendrin inhibition is a potential therapeutic strategy for overcoming diuretic resistance[19]. To identify an optimal pendrin inhibitor, I conducted small-molecule screening using the YFP fluorescence quenching assay. Among the candidate compounds, A4009 was selected as the most suitable for drug development and was subsequently used in my experiments. A4009 demonstrated less cytotoxicity even at higher concentrations compared to previously reported pendrin inhibitors (PDSinh-A01, PDSinh-C01), as confirmed in cytotoxicity assays. Additionally, Cl^-/HCO_3^- exchange experiments verified that A4009 exhibits a specific anion exchange activity. To confirm whether the diuretic effect of A4009 is specifically mediated through pendrin, I conducted diuretic experiments using pendrin KO animal models. In pendrin knockout models, the additive diuretic effect observed with the combination of furosemide and A4009 in wild-type animals was absent. Furthermore, the combined treatment led to increased urinary excretion of Na^+ and K^+ compared to furosemide alone. However, this increase was not observed in the pendrin knockout model, confirming that the diuretic effect of A4009 is specifically mediated by pendrin inhibition.

The expression of pendrin is regulated by multiple factors, including aldosterone, acid-base status, and RAAS activation. In this study, mRNA sequencing revealed that the expression of Rac1 and Nr3c2 (encoding the mineralocorticoid receptor, MR) was significantly increased, suggesting that both Rac1 and MR may contribute to the upregulation of pendrin. Previous research has shown that Rac1 can activate MR independently of aldosterone, promoting the nuclear translocation and transcriptional activity of MR and leading to increased expression of MR target genes[29, 30]. Consistently, in situ proximity ligation assays confirmed enhanced interaction between Rac1 and MR, supporting the activation of this signaling pathway in collecting duct cells. Rac1 has been shown to activate MR independently of aldosterone, thereby enhancing the transcription of MR target genes involved in sodium and chloride retention[29]. MR stimulation is known to increase pendrin expression and promote its apical localization, as

demonstrated in mineralocorticoid-treated models[11]. Furthermore, angiotensin II has been reported to increase pendrin expression via AT1a receptor and Rac1-dependent mechanisms, even in the absence of aldosterone[14, 31]. Taken together, these findings suggest that activation of Rac1–MR signaling under furosemide induced salt loss leads to increased pendrin expression, contributing to compensatory chloride reabsorption and the development of loop diuretic resistance[19, 32].

Pendrin has gained attention as a potential therapeutic target for hypertension. Previous studies reported that loss-of-function mutations in SLC26A4 are associated with reduced blood pressure in humans, and pendrin knockout mice show blunted hypertensive responses to angiotensin II. Consistently, treatment with the selective pendrin inhibitor A4009 lowered blood pressure in the angiotensin II-induced hypertension model[14, 31]. Angiotensin II-induced hypertension through vasoconstriction, sodium retention and fluid accumulation. In chronic kidney disease (CKD) and essential hypertension, the RAAS is known to be activated both systemically and intrarenally. In this study, A4009 treatment conferred a marked antihypertensive effect in angiotensin II-induced model, supporting the therapeutic potential of pendrin blockade in RAAS-driven hypertension.

Pendrin is also expressed in extra-renal tissues such as the inner ear and thyroid gland. However, in adults, the cochlea is fully developed, making the risk of ototoxicity due to pendrin inhibition relatively low[33, 34]. In contrast, the potential effects on thyroid function remain to be clarified in future clinical studies. In this study, A4009 selectively targeted SLC26A4 with minimal activity on other transporter families. According to its selectivity profile, A4009 may also inhibit SLC26A3 in addition to SLC26A4. SLC26A3 is reported to be abundant in the intestinal epithelium and functions in transepithelial Cl^-/HCO_3^- exchange in enterocytes. Inhibiting SLC26A3 can lead to side effects such as diarrhea in some patients. Therefore, the possibility of off-target effects on structurally similar transporters, such as SLC26A6, cannot be excluded and requires further validation[35, 36].

5. CONCLUSION

Pendrin inhibition by A4009 significantly improves diuretic outcomes in a model of diuretic resistance by preventing compensatory sodium reabsorption and enhancing the furosemide-induced excretion of sodium through urine. These finding suggest that pendrin inhibition represents a promising therapeutic approach to overcoming diuretic resistance by reducing sodium reabsorption. Additionally, a pendrin inhibitor was found to have an additional effect of reducing blood pressure in an angiotensin II-induced hypertension model. Future research should focus on evaluating the long-term efficacy, side effects, and clinical applicability of pendrin inhibitors as a novel class of diuretics.

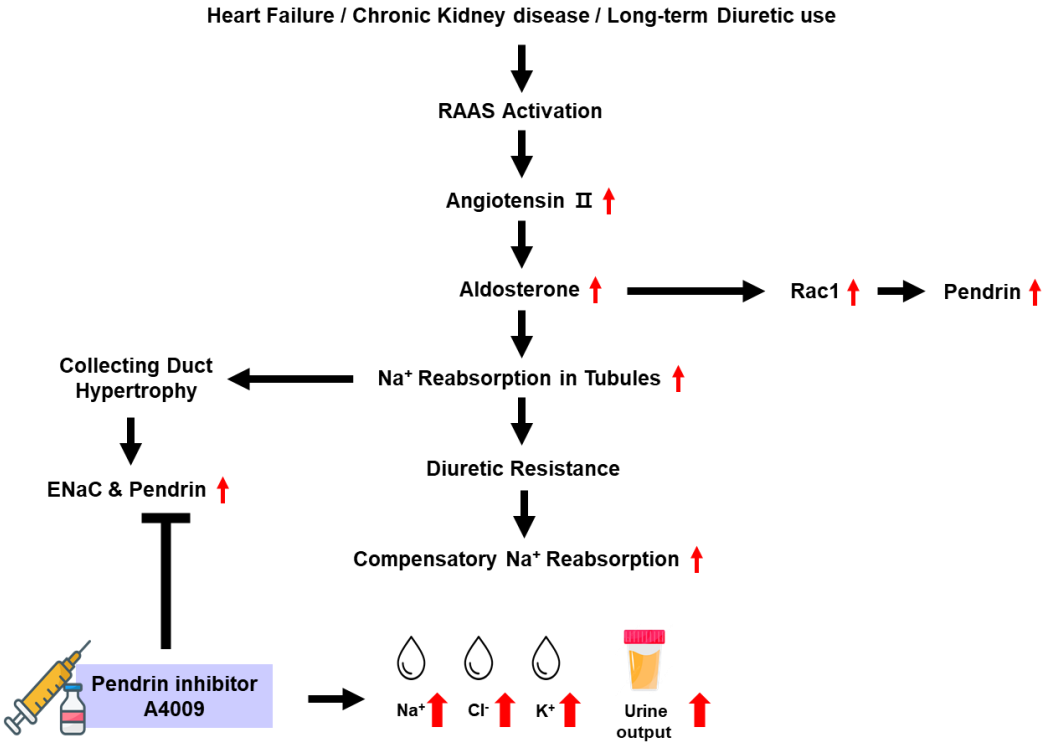

References

1 D. Pearce, R. Soundararajan, C. Trimpert, O. B. Kashlan, P. M. Deen, and D. E. Kohan, "Collecting duct principal cell transport processes and their regulation," (in eng), *Clin J Am Soc Nephrol,* vol. 10, no. 1, pp. 135-46, Jan 7 2015, doi: 10.2215/cjn.05760513.

2 C. A. Wagner *et al.*, "Regulation of the expression of the Cl-/anion exchanger pendrin in mouse kidney by acid-base status," (in eng), *Kidney Int,* vol. 62, no. 6, pp. 2109-17, Dec 2002, doi: 10.1046/j.1523-1755.2002.00671.x.

3 S. M. Wall, "Regulation of Blood Pressure and Salt Balance By Pendrin-Positive Intercalated Cells: Donald Seldin Lecture 2020," (in eng), *Hypertension,* vol. 79, no. 4, pp. 706-716, Apr 2022, doi: 10.1161/hypertensionaha.121.16492.

4 M. Soleimani *et al.*, "Pendrin: an apical $Cl^-/OH^-/HCO_3^-$ exchanger in the kidney cortex," (in eng), *Am J Physiol Renal Physiol,* vol. 280, no. 2, pp. F356-64, Feb 2001, doi: 10.1152/ajprenal.2001.280.2.F356.

5 Y. H. Kim *et al.*, "Immunocytochemical localization of pendrin in intercalated cell subtypes in rat and mouse kidney," (in eng), *Am J Physiol Renal Physiol,* vol. 283, no. 4, pp. F744-54, Oct 2002, doi: 10.1152/ajprenal.00037.2002.

6 I. E. Royaux *et al.*, "Pendrin, encoded by the Pendred syndrome gene, resides in the apical region of renal intercalated cells and mediates bicarbonate secretion," (in eng), *Proc Natl Acad Sci U S A,* vol. 98, no. 7, pp. 4221-6, Mar 27 2001, doi: 10.1073/pnas.071516798.

7 Q. Liu *et al.*, "Asymmetric pendrin homodimer reveals its molecular mechanism as anion exchanger," (in eng), *Nat Commun,* vol. 14, no. 1, p. 3012, May 25 2023, doi: 10.1038/s41467-023-38303-0.

8 L. Wang, A. Hoang, E. Gil-Iturbe, A. Laganowsky, M. Quick, and M. Zhou, "Mechanism of anion exchange and small-molecule inhibition of pendrin," (in eng), *Nat Commun,* vol. 15, no. 1, p. 346, Jan 6 2024, doi: 10.1038/s41467-023-44612-1.

9 S. M. Wall and Y. Lazo-Fernandez, "The role of pendrin in renal physiology," (in eng), *Annu Rev Physiol,* vol. 77, pp. 363-78, 2015, doi: 10.1146/annurev-physiol-021014-071854.

10 M. Soleimani, "The multiple roles of pendrin in the kidney," (in eng), *Nephrol Dial Transplant,* vol. 30, no. 8, pp. 1257-66, Aug 2015, doi: 10.1093/ndt/gfu307.

11 J. W. Verlander *et al.*, "Deoxycorticosterone Upregulates PDS (Slc26a4) in Mouse Kidney," *Hypertension,* vol. 42, no. 3, pp. 356-362, 2003/09/01 2003, doi: 10.1161/01.HYP.0000088321.67254.B7.

12 C. S. Wilcox, J. M. Testani, and B. Pitt, "Pathophysiology of Diuretic Resistance and Its Implications for the Management of Chronic Heart Failure," (in eng), *Hypertension,* vol. 76, no. 4, pp. 1045-1054, Oct 2020, doi: 10.1161/hypertensionaha.120.15205.

13 Z. L. Cox *et al.*, "Compensatory post-diuretic renal sodium reabsorption is not a dominant mechanism of diuretic resistance in acute heart failure," (in eng), *Eur Heart J,* vol. 42, no.

43, pp. 4468-4477, Nov 14 2021, doi: 10.1093/eurheartj/ehab620.

14 J. W. Verlander *et al.*, "Angiotensin II acts through the angiotensin 1a receptor to upregulate pendrin," (in eng), *Am J Physiol Renal Physiol,* vol. 301, no. 6, pp. F1314-25, Dec 2011, doi: 10.1152/ajprenal.00114.2011.

15 N. Xu *et al.*, "Hypokalemia and Pendrin Induction by Aldosterone," *Hypertension,* vol. 69, no. 5, pp. 855-862, 2017/05/01 2017, doi: 10.1161/HYPERTENSIONAHA.116.08519.

16 R. L. Sutliff *et al.*, "Contractile force is enhanced in Aortas from pendrin null mice due to stimulation of angiotensin II-dependent signaling," (in eng), *PLoS One,* vol. 9, no. 8, p. e105101, 2014, doi: 10.1371/journal.pone.0105101.

17 M. Vallet *et al.*, "Pendrin regulation in mouse kidney primarily is chloride-dependent," (in eng), *J Am Soc Nephrol,* vol. 17, no. 8, pp. 2153-63, Aug 2006, doi: 10.1681/asn.2005101054.

18 H. Amlal and M. Soleimani, "Pendrin as a novel target for diuretic therapy," (in eng), *Cell Physiol Biochem,* vol. 28, no. 3, pp. 521-6, 2011, doi: 10.1159/000335117.

19 O. Cil, P. M. Haggie, P. W. Phuan, J. A. Tan, and A. S. Verkman, "Small-Molecule Inhibitors of Pendrin Potentiate the Diuretic Action of Furosemide," (in eng), *J Am Soc Nephrol,* vol. 27, no. 12, pp. 3706-3714, Dec 2016, doi: 10.1681/asn.2015121312.

20 J. Jung *et al.*, "The HSP70 co-chaperone DNAJC14 targets misfolded pendrin for unconventional protein secretion," (in eng), *Nat Commun,* vol. 7, p. 11386, Apr 25 2016, doi: 10.1038/ncomms11386.

21 E. H. Lee *et al.*, "Inhibition of Pendrin by a small molecule reduces Lipopolysaccharide-induced acute Lung Injury," (in eng), *Theranostics,* vol. 10, no. 22, pp. 9913-9922, 2020, doi: 10.7150/thno.46417.

22 O. Söderberg *et al.*, "Direct observation of individual endogenous protein complexes in situ by proximity ligation," (in eng), *Nat Methods,* vol. 3, no. 12, pp. 995-1000, Dec 2006, doi: 10.1038/nmeth947.

23 E. J. Hoorn and D. H. Ellison, "Diuretic Resistance," (in eng), *Am J Kidney Dis,* vol. 69, no. 1, pp. 136-142, Jan 2017, doi: 10.1053/j.ajkd.2016.08.027.

24 V. Vallon, J. Schroth, F. Lang, D. Kuhl, and S. Uchida, "Expression and phosphorylation of the Na+-Cl− cotransporter NCC in vivo is regulated by dietary salt, potassium, and SGK1," (in eng), *Am J Physiol Renal Physiol,* vol. 297, no. 3, pp. F704-12, Sep 2009, doi: 10.1152/ajprenal.00030.2009.

25 J. Hadchouel, D. H. Ellison, and G. Gamba, "Regulation of Renal Electrolyte Transport by WNK and SPAK-OSR1 Kinases," (in eng), *Annu Rev Physiol,* vol. 78, pp. 367-89, 2016, doi: 10.1146/annurev-physiol-021115-105431.

26 G. Gamba, "The thiazide-sensitive Na+-Cl− cotransporter: molecular biology, functional properties, and regulation by WNKs," (in eng), *Am J Physiol Renal Physiol,* vol. 297, no. 4, pp. F838-48, Oct 2009, doi: 10.1152/ajprenal.00159.2009.

27 B. B. Lins, F. A. M. Casare, F. F. Fontenele, G. L. Gonçalves, and M. Oliveira-Souza, "Long-Term Angiotensin II Infusion Induces Oxidative and Endoplasmic Reticulum

Stress and Modulates Na(+) Transporters Through the Nephron," (in eng), *Front Physiol,* vol. 12, p. 642752, 2021, doi: 10.3389/fphys.2021.642752.

28 C. A. Wagner, O. Devuyst, S. Bourgeois, and N. Mohebbi, "Regulated acid-base transport in the collecting duct," (in eng), *Pflugers Arch,* vol. 458, no. 1, pp. 137-56, May 2009, doi: 10.1007/s00424-009-0657-z.

29 S. Shibata, K. Ishizawa, and S. Uchida, "Mineralocorticoid receptor as a therapeutic target in chronic kidney disease and hypertension," *Hypertension Research,* vol. 40, no. 3, pp. 221-225, 2017/03/01 2017, doi: 10.1038/hr.2016.137.

30 N. Ayuzawa and T. Fujita, "The Mineralocorticoid Receptor in Salt-Sensitive Hypertension and Renal Injury," (in eng), *J Am Soc Nephrol,* vol. 32, no. 2, pp. 279-289, Feb 2021, doi: 10.1681/asn.2020071041.

31 T. D. Pham *et al.*, "Angiotensin II acts through Rac1 to upregulate pendrin: role of NADPH oxidase," (in eng), *Am J Physiol Renal Physiol,* vol. 326, no. 2, pp. F202-f218, Feb 1 2024, doi: 10.1152/ajprenal.00139.2023.

32 V. Pech, Y. H. Kim, A. M. Weinstein, L. A. Everett, T. D. Pham, and S. M. Wall, "Angiotensin II increases chloride absorption in the cortical collecting duct in mice through a pendrin-dependent mechanism," (in eng), *Am J Physiol Renal Physiol,* vol. 292, no. 3, pp. F914-20, Mar 2007, doi: 10.1152/ajprenal.00361.2006.

33 A. A. Dror, D. R. Lenz, S. Shivatzki, K. Cohen, O. Ashur-Fabian, and K. B. Avraham, "Atrophic thyroid follicles and inner ear defects reminiscent of cochlear hypothyroidism in Slc26a4-related deafness," (in eng), *Mamm Genome,* vol. 25, no. 7-8, pp. 304-16, Aug 2014, doi: 10.1007/s00335-014-9515-1.

34 P. Wangemann *et al.*, "Loss of cochlear HCO_3^- secretion causes deafness via endolymphatic acidification and inhibition of Ca2+ reabsorption in a Pendred syndrome mouse model," *American Journal of Physiology-Renal Physiology,* vol. 292, no. 5, pp. F1345-F1353, 2007, doi: 10.1152/ajprenal.00487.2006.

35 M. N. Chernova *et al.*, "Functional comparison of mouse slc26a6 anion exchanger with human SLC26A6 polypeptide variants: differences in anion selectivity, regulation, and electrogenicity," (in eng), *J Biol Chem,* vol. 280, no. 9, pp. 8564-80, Mar 4 2005, doi: 10.1074/jbc.M411703200.

36 Q. Yu, "Slc26a3 (DRA) in the Gut: Expression, Function, Regulation, Role in Infectious Diarrhea and Inflammatory Bowel Disease," (in eng), *Inflamm Bowel Dis,* vol. 27, no. 4, pp. 575-584, Mar 15 2021, doi: 10.1093/ibd/izaa256.

ABSTRACT

새로운 이뇨제 전략으로서의 펜드린 억제제: 이뇨제 저항성 및 안지오텐신 II 유도성 고혈압 표적 치료

배경: Pendrin(SLC26A4)은 신장에서 염화나트륨(NaCl)과 수분 재흡수에 중요한 역할을 하는 음이온 교환체입니다. 이는 집합관의 연결 세뇨관(connecting tubule)과 피질 집합관(cortical collecting duct)의 β-세포와 non-A/non-B 세포의 세포 꼭대기막(apical membrane)에 위치하고 있습니다. Pendrin은 주로 염화이온(Cl^-) 재흡수와 중탄산염(HCO_3^-) 분비를 Cl^-/HCO_3^- 교환을 통해 조절하며, 상피 나트륨 채널(ENaC) 및 Na^+-driven Cl^-/ HCO_3^- 교환체(NDCBE)를 간접적으로 조절하여 나트륨 재흡수에도 영향을 미칩니다. 최근 연구에서는 pendrin과 Na-K-Cl 공동수송체(NKCC2) 간의 상호작용이 밝혀졌으며, 이 두 수송체를 동시에 억제하면 강력한 이뇨 효과가 나타나는 것으로 보고되었습니다. 본 연구는 pendrin 발현이 증가된 조건에서 신규 pendrin 억제제가 이뇨제 저항성에 미치는 영향을 평가하고자 하였습니다. 또한, Angiotensin II 유도 모델을 이용하여 Angiotensin II의 역할을 분석하고, furosemide와 pendrin 억제제의 병용 이뇨 효과를 평가하여 치료적 전략 가능성을 탐색하고자 하였습니다.

방법: A4009를 처리 후, pendrin을 과발현시킨 PANC-1 세포에서 pH-sensitive fluorescent dye을 이용하여 in vitro Cl^-/HCO_3^- 교환 활성을 측정하였다. 이뇨 효과는 정상 생쥐, furosemide 저항성 모델, Angiotensin II 유도 고혈압 모델에서 평가되었고, A4009 단독 및 furosemide 병용 투여 후 소변량과 전해질 배설량을 측정하였습니다. Angiotensin II 모델에서는 혈압도 함께 측정하였습니다. 또한 각 동물 모델에서 pendrin 경로 활성화의 분자적 기전을 규명하기 위해 나트륨 수송체 및 조절 인자의 mRNA 및 단백질 발현을 정량적 실시간 PCR(qPCR)과 Western blot 분석을 통해 정량 평가하였습니다. 또한, pendrin과 신호전달 관련 단백질 간의 상호작용을 확인하기 위해 Proximity Ligation Assay (PLA)과 mRNA sequencing을 수행하였다.

결과: 신규 pendrin 억제제인 A4009는 in vitro 스크리닝을 통해 발굴되었으며, Cl^-/I^- 및 Cl^-/ HCO_3^- 교환에 대한 억제 효과는 각각 IC_{50} 59.5 ± 12.8 nM 및 52.6 ± 15.7 nM으로 나타났습니다. 정상 생쥐에서는 furosemide와 A4009 병용 시 용량 의존적으로 소변량이 유의미하게 증가하였고, Na^+, Cl^-, K^+ 배설이 증가하며, 소변 삼투압이 유의미하게 감소하였습니다. Furosemide 저항성 모델에서는 A4009 단독 투여가 소변량을 다소 증가시켰고, 병용 투여는 소변량과 Na^+, Cl^-, K^+ 배설을 증가시키고, 소변 삼투압을 유의미하게 감소시켰습니다. 이는 Angiotensin II에 의해 유도된 Rac1의 활성화가 MR의 전사 조절 및 pendrin 유전자 발현 증가에 관여함을 시사하며, Rac1–MR–pendrin 경로의 작동 가능성을 뒷받침한다. Angiotensin II 유도 고혈압 모델에서 A4009의 이뇨 효과가 확인

되었습니다. A4009 단독 투여는 소변량과 Na^+, K^+, Cl^- 배설에 유의미한 영향을 미치지 않았으나, furosemide와 병용 투여 시 소변량과 전해질 배설이 유의미하게 증가하고, 소변 삼투압은 감소하였습니다. A4009는 단독으로도 고혈압 생쥐의 혈압을 감소시켰으며, pendrin 억제가 이뇨 반응을 증강시키고 고혈압 상태에서 혈압을 낮추는 데 기여할 수 있음을 시사합니다.

결론: 본 연구는 pendrin 억제가 Angiotensin II 유도 고혈압 및 이뇨제 저항성 조건에서 나트륨 및 수분 저류를 완화하는 데 효과적일 수 있음을 제시합니다. pendrin 발현이 증가된 조건에서 pendrin 억제제가 새로운 이뇨제 후보로서의 가능성을 강조합니다. 향후 연구는 pendrin 과발현 모델에서 A4009의 장기적인 안전성, 효능, 그리고 임상적 적용 가능성을 추가적으로 평가하고, 다양한 병리적 조건에서의 치료적 응용 가능성을 탐색해야 합니다.

Keywords: diuretic, diuretic resistance, RAAS system, Pendrin, Angiotensin II